EFFECTS OF STRAIN ENERGY RELEASE RATE ON DELAMINATION IN TEMPERATURE ENVIRONMENT

by

VENKATA NAGA RAVITEJ SANKARABATLA

Presented to the Faculty of the Graduate School of

The University of Texas at Arlington in Partial Fulfillment

of the Requirements

for the Degree of

MASTER OF SCIENCE IN AEROSPACE ENGINEERING

THE UNIVERSITY OF TEXAS AT ARLINGTON

AUGUST 2013

Acknowledgments

First, I would like to express my sincere gratitude to my professor and supervisor, Dr. Wen S Chan, whose knowledge horizon and acumen added a significant value to my entire tenure at the university. His expertise, conscientious guidance and unparalleled support have enabled me to grow up the learning curve. It was an honor to work under his mentorship. He has been highly encouraging throughout my master's program at the university. I feel blessed and obliged to be associated with him for this research work.

I would also like to thank the rest of my thesis committee: Dr. Nomura Seiichi, Dr. Adnan Ashfaq, for their constant encouragement and timely insights.

I would like to thank my mother and father for their love and support during my odyssey in Arlington. I would like to convey my best regards to all my friends both from the University of Texas at Arlington and the Institute of Aeronautical Engineering who are well established across the globe, for all their confidence in me and encouragement they provided.

I'd like to appreciate Shiva Kumar Samala, Pavan Nuthi and Anudeep Palanki for their valuable suggestions and personal support offered during the project's documentation phase. Last but not the least; I would like to highlight the efforts of my close friend Ramesh Sharma who provided his expert opinion, honest feedback and encouragement for my final presentation.

JULY 26, 2013

ABSTRACT

EFFECTS OF STRAIN ENERGY RELEASE RATE ON DELAMINATION IN TEMPERATURE ENVIRONMENT

Venkata Naga Ravitej Sankarabatla, M.S

The University of Texas at Arlington, 2013

Supervising Professor: Wen S Chan

Delamination is the weakest and major failure mode in laminated composites. Extensive efforts on initiation and growth of delamination under mechanical load have been investigated.

A little emphasis was made earlier to account for the delamination in laminates under temperature loading. Strain energy release rate, a fracture mechanics parameter has been widely accepted to use for study the characteristics of delamination growth. In order to conduct a quick assessment of delamination growth, a closed form expression for double cantilever beam is developed to quantify the strain energy release rate of the laminate subjected to temperature environment.

A finite element model is also developed to use for validating the analytical expression. A parametric study is also conducted to study the effects of strain energy release rate with percentage of angle ply variation in $[0_2/\pm\theta_3/\mp\theta_3/0_2]_s$

Table of Contents

List of Illustrations

List of Tables

Chapter 1

Introduction

1.0 Background and Past Work

A structural composite is fundamentally a combination of fibers and matrix amalgamated in an appropriate ratio whose mechanical properties and performance are designed to be superior to those of the constituent materials acting together. One of the phases is usually stiffer and stronger called the reinforcement while the weaker phase is called the matrix which is used to provide the binding the two phases together. The fibers will provide the required strength and stiffness and the matrix provides the lateral support of the fibers. Uniquely, these fibers can be oriented in any direction with respect to the material system. The geometry, the orientation as well as the distribution of the reinforcement strongly influences the mechanical and thermal properties of the composite material.

1.1 Delamination

Polymeric fiber reinforced composites have been widely accepted for primary structures in newly developed aircrafts and aerospace vehicles such as Airbus 380[1], Boeing 787[2], etc. The aerospace industry is widely expanding its frontiers in the field of composites. This is primarily due to advantages of composite materials such as high corrosion resistance and high specific stiffness/or high specific strength along the fiber direction. To take these advantages composite structures are made of laminating a sequence of thin layers together and those layers are oriented along the required direction of loading.

However, any composite structure cannot be attributed with a positive note as there are some disadvantages which hold a unique feature i.e. the separation between the layers namely delamination. Since composite structures are made of laminating a sequence of thin layers together, there is no reinforcement in the thickness direction of the structured laminates.

Interestingly the reinforcement in thickness direction cannot be sustained as this would ruin the laminate during the manufacturing process and also there exists a numerous factors which have adverse effects on delamination. Practically, complete elimination of delamination from a structure is impossible. So, as a design engineer the possibility is to minimize the effects on the complex structures reducing the delamination by manipulating other factors and hence increasing the fatigue life of structure

Delamination is one of the primary failure modes of laminated composite structures. Presence of delamination in composite structures will result in reduction of strength, stiffness as well as fatigue life. Its growth can lead to the total failure of the structure. Hence, understanding mechanism of delamination characteristics such as onset and growth becomes one of the important tasks in design. To quantify these behaviors of delamination, fracture mechanics is a common tool used in study. .

Extensive studies on characteristics of delamination initiation and growth have been conducted. Some of pioneer works in this area have been collected in the book by Newaz [1]. In study of double cantilevered beam, Whitney [2] examined the area method of loading curve used to obtain the Mode I fracture resistance. Wang and Crossman[3] investigated on the initiation and growth of transverse cracks and edge delamination in composite laminates and formulated a theory based on the classical linear fracture mechanics concept of strain energy release rate as a criterion for crack growth and incorporated virtual crack closure technique to generate numerical results. In Obrien, et.al [4] studied laminated plate theory analysis to calculate the strain energy release rate associated with edge delamination growth in a composite laminate. The analysis includes the contribution of residual thermal and moisture stresses to the strain energy released. The strain energy release rate, G, increased when residual thermal effects were combined with applied mechanical strains, but then decreased when increasing moisture content was included. A quasi-three-dimensional finite element analysis indicated identical trends and demonstrated

these same trends for the individual strain energy release rate components, G_I and G_{II}, associated with inter-laminar tension and shear. An experimental study indicated that for T300/5208 graphite-epoxy composites, the inclusion of residual thermal and moisture stresses did not significantly alter the calculation of inter-laminar fracture toughness from strain energy release rate analysis of edge delamination data taken at room temperature, ambient conditions. Later, Chan and Wang [5] highlighted the major effects of a 90° ply on matrix cracks and edge delamination in composite materials. They identified that when a toughened 90° ply serving as the core layer in cross plied and angle plied laminates, has a definite effect on the matrix and the threshold delamination in the laminate.

1.2 Application of Fracture Mechanics to Delamination

1.2.1 Stress Intensity Factor and Crack Tip Stress Singularity:

It is well known that stress near crack tip gives rise a steep stress gradient with a $1/\sqrt{r}$ singularity for isotropic linear elastic materials. Stress intensity factor is used to quantify this highly stress gradient. To evaluate the energy required to form a new crack surface, strain energy release rate is often used. The energy release rate near a crack tip of an isotropic linear elastic material has been found to be related wit stress intensity factor. For a crack presence in composite laminate, the order of stress singularity due to presence of a crack is not only function of material constants but also stacking sequence of the laminate. Hence, to avoid determining the order of singularity strain energy release rate is often used in fracture analysis for composite materials.

1.2.2 Strain Energy Release Rate:

It is defined as “the energy dissipated during the crack formation for a newly created crack surface area” and denoted as G. It is a very primitive factor in fracture mechanics because the energy that must be supplied to the crack tip to grow must be balanced by the amount of

energy dissipated due to formation of new surface. Further Definition of strain energy release rate will be discussed in Chapter 2.

1.3 Outline of Thesis

This thesis is intended to present the effects of the strain energy release rates on the delamination of the laminated composite structure in a temperature environment. The first chapter briefly describes the critical failure mode, delamination, in laminated composite structures. The past work in the field of delamination collected in the book which contributed to attain some fundamental knowledge in the concept of strain energy release rate was mentioned. Thoroughly understanding the mechanics involved in the process of delamination we move on to chapter two, which primarily focuses on the underlying concepts explained in previous chapter to derive a valid expression to explain the delamination in composite beams namely double cantilever beam subjected to normal mechanical loading and also with elevation in temperature. This chapter enlightens more on the physical concepts of the fracture mechanics and details out the derivation in order to understand its form when compared to some standard physical phenomenon. The chapter three is the essence of this thesis explaining the necessity for understanding the advantages of using a finite element analysis and elucidating the concept of delamination in a technique where it justifies the imagination and validates the physical principle derived previously in chapter two. A finite element analysis would assist to validate some principles which are drafted on same methodologies but using different platforms. An ANSYS 12.1 analysis platform is preferred to perform the task which abetted to visualize the delamination in temperature environment. Chapter four performs parametric study on the current problem in various cases. This chapter is of core importance demonstrating the influence of several other factors like stacking sequence, material properties and temperature variation on the delamination predicting a particular pattern for this variation. It also throws some light on the variation of strain energy release rate with ply angle keeping the rest of the sequence same. Chapter five deals mainly

explaining the observations made by analyzing the results obtained and detailing out the reasons behind the values attained from both the finite element analysis and the analytical formulations predicting the differences in the expected and achieved values. Chapter six is a concluding chapter dealing mostly with the idea presenting the gist of the thesis numerically, the conclusions made from the complete research and gives the scope for further enhancing the concept by putting forth some new ideas which can take this research work ahead.

Chapter 2

Calculations Pertaining to Strain Energy Release Rate using Energy Method

2.1 Strain Energy Release Rate

The strain energy release rate is a fracture parameter which is used to measure delamination characteristics of composite laminates. In this chapter an extensive study on the effects on delamination in a composite double cantilevered beam is performed in the temperature environment.

For a structure with a crack, the strain energy release rate (G) is defined as the amount of energy released in order to extend the crack and is mathematically given by

$$G = \frac{\partial W}{\partial a} - \frac{\partial U}{\partial a} \tag{2.1}$$

Where W is the external work done, U is the internal strain energy and A is the crack surface.

Let consider a cantilevered beam subjected to a load, P as shown in Figure 2.1.

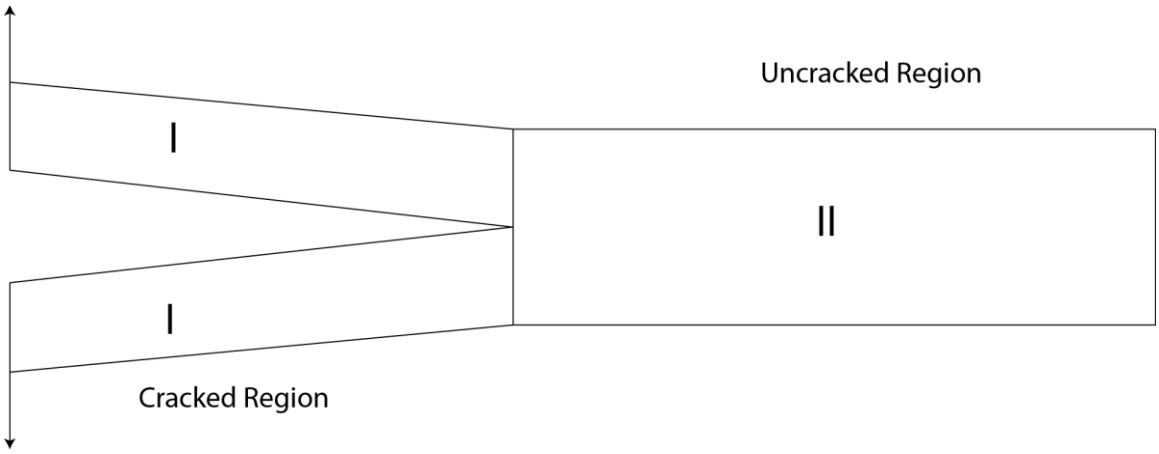

Figure 2.1 Double Cantilever Beam with Load

The external work done (W) is given by

$$W = P.\delta \tag{2.2}$$

And strain energy is given by

$$U = \frac{1}{2} P.\delta \tag{2.3}$$

-Where δ is the displacement at the load. Hence, for a constant load application, we have

$$W = 2U \tag{2.4}$$

Therefore Equation (1) can be rewritten as

$$G = \frac{\partial U}{\partial a} \tag{2.5}$$

The Double Cantilever Beam (DCB) is used to access the mode I failure strength of composite laminate with all 0^0 plies. In this type of failure mode, the load is applied on the cantilever arms and the crack propagates in the direction perpendicular to the applied load. In this case, no shear at the crack tip of delamination exists. Hence, the crack growth is due to the out-of-plane load. For this crack growth, we term as “Mode-I” fracture. When the crack advances, the debonding takes place between the interfacial surfaces leading to the fracture, releasing the energy which is resulting in delamination. The energy that is dissipated in this process is coined as strain energy release rate or fracture energy pertaining to the DCB. During this process of crack propagation, the applied load will assist in increasing the energy associated with the cantilever arms and thus succeeds in attaining an energy level which is equal to or greater than the threshold barrier energy. If the laminate of the beam contains angle plies besides 0^0 plies,

there exists shear stress at the neighborhood of crack. As result, the fracture mode of this laminate is not a pure “mode I”. It is mixed mode fracture.

The strain energy release mechanism is controlled at least partially by the structural interaction between plies during loading the laminate. Since this interaction can be altered by the kinematics of the crack, the energetic argument provides not only a criterion for crack growth but also for the kinematic effects such as growth stability.

In major context, every beam will be associated with the particular strain energy release rate called critical strain energy release rate (G_C). This critical strain energy is based on material properties, geometry and type of specimen. When a load is applied the energy will be stored in the form of strain energy initiating the growth of crack. As a result the strain energy is varying from one nodal point to the other. This strain energy differences will result in the release of energy to increase the surface area of the crack called strain energy release rate and this energy is associate with the loading conditions and boundary conditions irrespective of specimen and it is termed as available strain energy (G_F).

The growth of the delamination is initially stable i.e the applied load must be increased in order to extend the crack. The specimen will offer a material resistance against the ply delamination for the applied load. This quantity is measured by critical strain energy release rate G_C. During a stable growth process the stressed plies will release strain energy when a new crack surface is created due to the applied load. The rate of available energy released per unit crack surface is obtained from G_F, which is considered as a driving force which can further extend the crack when $G_F=G_C$.

If $G_F < G_C$ the crack will still remain in its stationary state until the applied load is increased, whereas the crack growth becomes unstable when $G_F > G_C$. The available strain energy is a complicated function of ply properties, ply thickness, ply sequence, crack size, crack geometry and crack location.

However, adopting a double cantilever beam (DCB) for the delamination analysis will be very convenient but with few assumptions which make the complex analysis a simpler one and they are:

- The crack front is always linear and the properties of linear elastic fracture mechanics are applicable.
- The crack investigation is based on inter-ply cracks namely delamination.
- The crack will not jump from one interface to other.
- The shear effects of loading on the crack are neglected.
- The nonlinearities in the material may exist but for the simplicity case the material properties are assumed to be same as initial and analysis is always static crack propagation.
- Initial crack length, size and number of cracks are presumed to be known.
- The analysis which includes thermal effects considers uniform temperature applied.
- In case of thermal loading, the effect of forces and moments are considered only in X-direction for ease of evaluation of strain energy.

With the understanding of a double cantilever beam (DCB), this theory is extended to cracks under temperature loading. The idea is to understand the behavior of cracks and their stability and growth in a temperature environment. The bottom line is to evaluate a criterion for the crack behavior. For example, during a curing process the laminate undergoes a series of changes in temperature as well as pressure in an auto clave which can affect the laminate if there are cracks present in the layup. So, the effects of temperature on crack propagation will be studied and the analytical analysis will be provided in the further sections.

The following section is to describe how U (strain energy) is evaluated.

2.2 Strain Energy Release Rate of DCB with General Layup

2.2.1 Mechanical Loading without Temperature

A DCB specimen shown in fig 2.2 is divided by crack region (region I) and uncrack region (Region II).

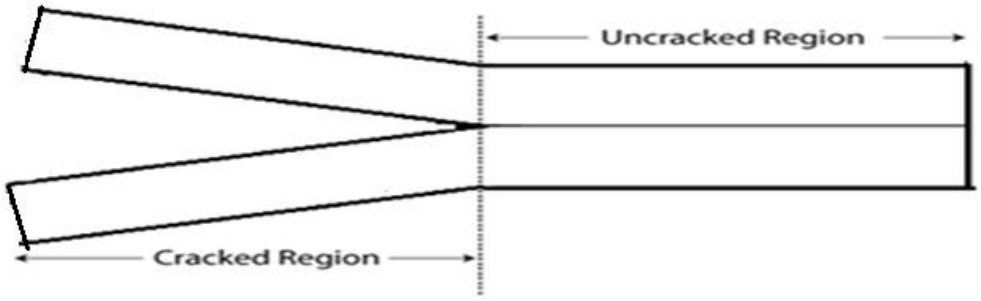

Fig 2.2 Cracked and Uncracked

Taking free body diagram at the crack tip as shown in Figure 2.3, it shows the applied load induced a moment at the crack tip in region I. Both load and moment at crack tip area of region II are self-balanced, resulting in no existence of load application in region II.

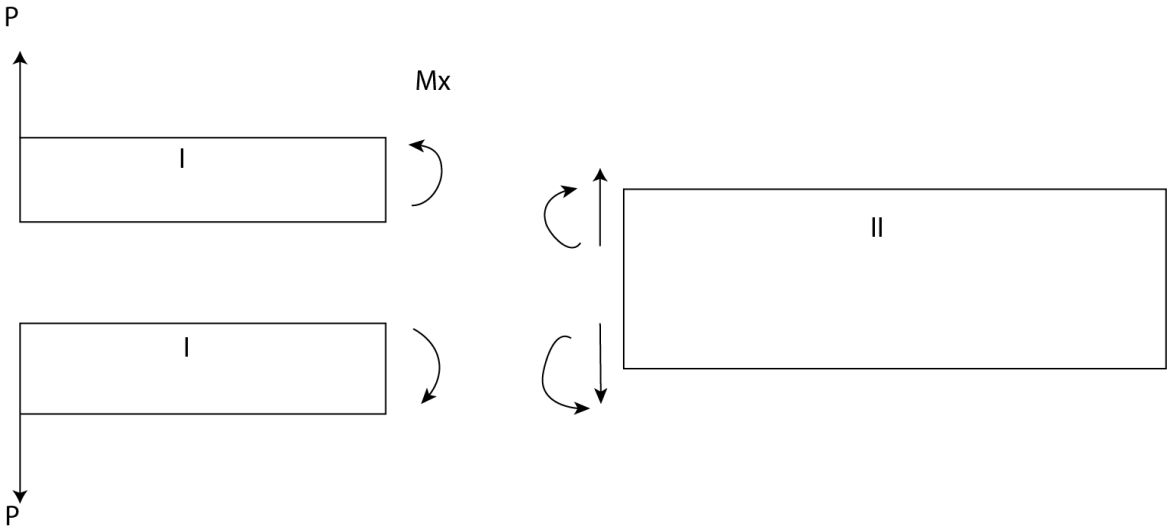

. Fig 2.3 Free Body Diagram of Beam without Temperature

From strength of materials concept, total strain energy, U for a beam can be expressed as

$$U = \frac{1}{2}\int_0^L \frac{M^2}{EI}dx \tag{2.6}$$

For a Laminated Beam

$$\mathrm{U} = \frac{1}{2}\int_0^{\mathrm{L}} d_{11}^{I} M^2 dx \tag{2.7}$$

Where d_{11}^{I} is flexibility of laminate of Region I

$$U_{II} = 0$$

Strain Energy for both regions will be,

$$G = 2\frac{\partial U_I}{B\partial a}$$

It should be mentioned that “B” is the width of laminate.

$$M_X = P.x$$

Therefore,

$$G = \frac{d_{11}^{I}.P^2.a^2}{B} \tag{2.8}$$

2.2.2 Mechanical Loading with Temperature

Whenever a composite laminate is subjected to mechanical as well as thermal loading, the forces and moments acting on it are

$$N_x, M_x, N_x^T, M_x^T, N_y, M_y, N_y^T, M_y^T, N_{xy}, M_{xy}, N_{xy}^T, M_{xy}^T$$

Since we are applying the load only in the direction perpendicular to the crack surface typically being Mode I the other forces acting on the beam are neglected. The thermal forces and moments generated due to the elevated temperature will act accordingly.

Predominantly, N_x^T & M_x^T are contributing majorly for

For a DCB with Temperature Loading of ΔT,

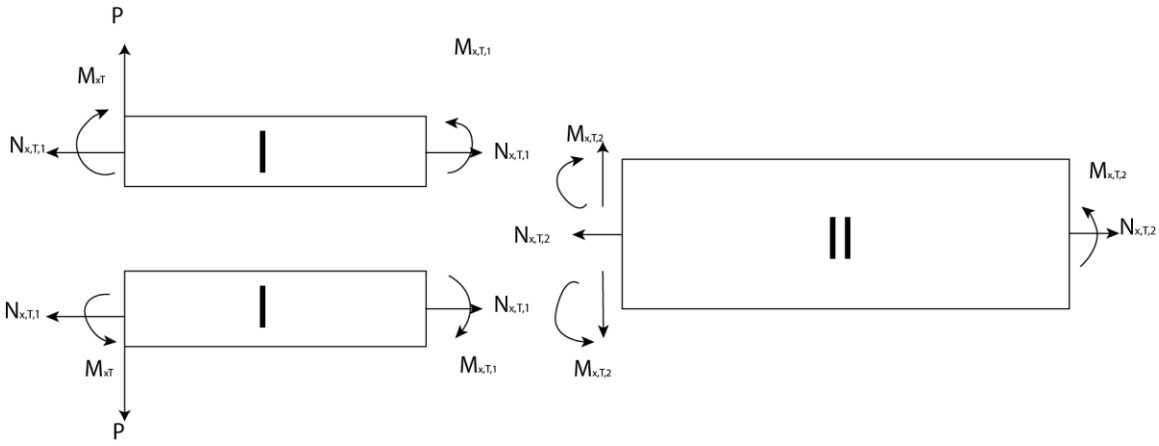

Fig 2.4 Illustration for Delamination

The Double Cantilever Beam experiences stresses due to bending and axial loads. So, we need to consider the strain energy due these loads.

Strain energy due to Bending,

Region I,

$$U_b^I = d_{11}^I \int_0^a (Px + B.M_{x,I}^T)^2 dx$$

$$U_b^I = \frac{d_{11}^I}{2} . \frac{1}{3P} . [(Pa + BM_{x,I}^T)^2 - (BM_{x,I}^T)^2] \quad (2.9)$$

Region II,

$$U_b^{II} = \frac{d_{11}^{II}}{2}\int_a^L (BM_{x,II}^T)^2 dx$$

$$U_b^{II} = \frac{d_{11}^{II}}{2}(BM_{x,II}^T)^2.(L-a) \tag{2.10}$$

Strain energy due to axial load,

Region I,

$$U_a^{II} = \frac{1}{2EA_I}\int_0^a (BN_{x,I}^T)^2 dx$$

$$U_a^{II} = \frac{a_{11}^I}{2}(BN_{x,I}^T)^2.a \tag{2.11}$$

Region II,

$$U_a^{II} = \frac{1}{2EA_{II}}\int_a^L (BN_{x,II}^T)^2 dx$$

$$U_a^{II} = \frac{a_{11}^{II}}{2}\int_a^L (BN_{x,II}^T)^2 (L-a) \tag{2.12}$$

Therefore,

$$G = \frac{1}{B}\frac{\partial U}{\partial a}$$

$$G = \frac{1}{B}\{d_{11}^I (Pa + BM_{x,I}^T)^2 + a_{11}^I (BN_{x,I}^T)^2 - \frac{d_{11}^{II}}{2}(BM_{x,II}^T) - \frac{a_{11}^{II}}{2}(BN_{x,II}^T)^2\} \tag{2.13}$$

(Mixed –Mode fracture)

Examining the above equation, the $M^{T}_{x,II} = 0$, if the laminate is symmetrical. The energy term due to temperature involved multiplying a_{11} of the laminate in each region. Because of magnitude of $a_{11,}$ effect of temperature contributes to G will be small.

Chapter 3

Finite Element Modeling

A finite element analysis would support the analytical argument strongly and with the latest developments in analysis software's like Ansys™ and Abaqus™ will help to understand and establish a relation between analytical and FEA approach. ANSYS™ is used to develop a FEM model in this research. Modeling delamination in ANSYS™ requires a lot of body work. Pre dominantly there are two techniques that are widely used in modeling delamination. They are:

- Virtual Crack Closure technique (VCCT)
- Cohesive Zone Modeling (CZM)

Apparently both these techniques have become very popular in industries over the years. There few more techniques which can be implemented but the results obtained from VCCT and CZM have shown more compliance with the experimental analysis.

However, even these two techniques have their own weaknesses as well, but the choice over the selection of techniques is subjected to the constraints like loading, element type, analysis, boundary conditions, etc.

3.1 Virtual Crack Closure Technique (VCCT):

VCCT calculates G, with the assumption that the energy needed to separate the surface is same as the energy needed to close the same surface area. This technique uses a contact or interfacial elements along a predefined interface of model.

Nevertheless, this type of modeling involves a fracture mechanics technique with large body work. Although the growth criterion is energy release rate, G which is the subject of interest but there are few assumptions that must be accounted for, before proceeding to model. They are

- Number of cracks
- Location of cracks
- Size of cracks

Also, the analysis is arduous whenever the type of structure and loading are complex.

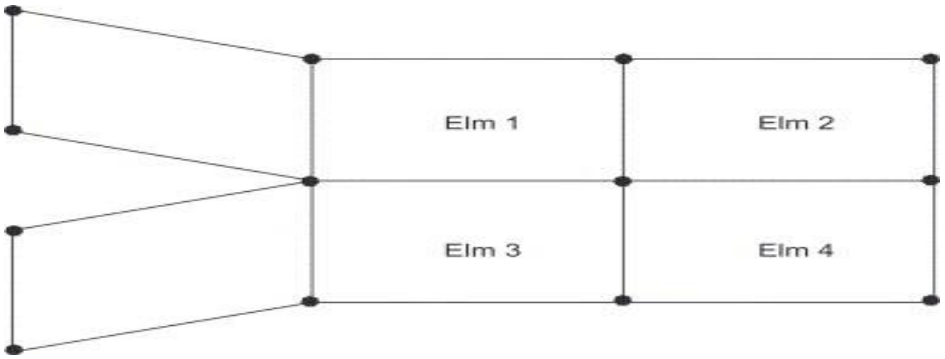

Figure 3-1 VCCT model with crack tip and elements

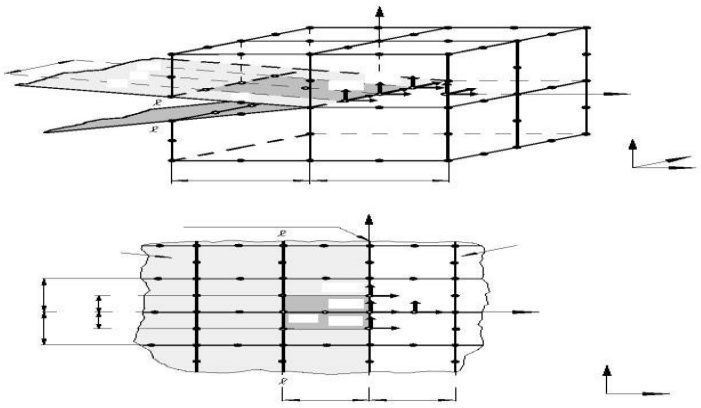

Figure 3-2 A 3-D VCCT model with crack front

In 1956, Irwin [6] considered an infinite plate with fixed ends containing a crack size a. If the forces applied to the crack edge are sufficient to close the crack over an infinitesimal distance as shown in Figure 3-3, then work will be done during the crack closure. If the process is reversed, then work will be released from the plate. This realization led to another definition of strain energy release rates.

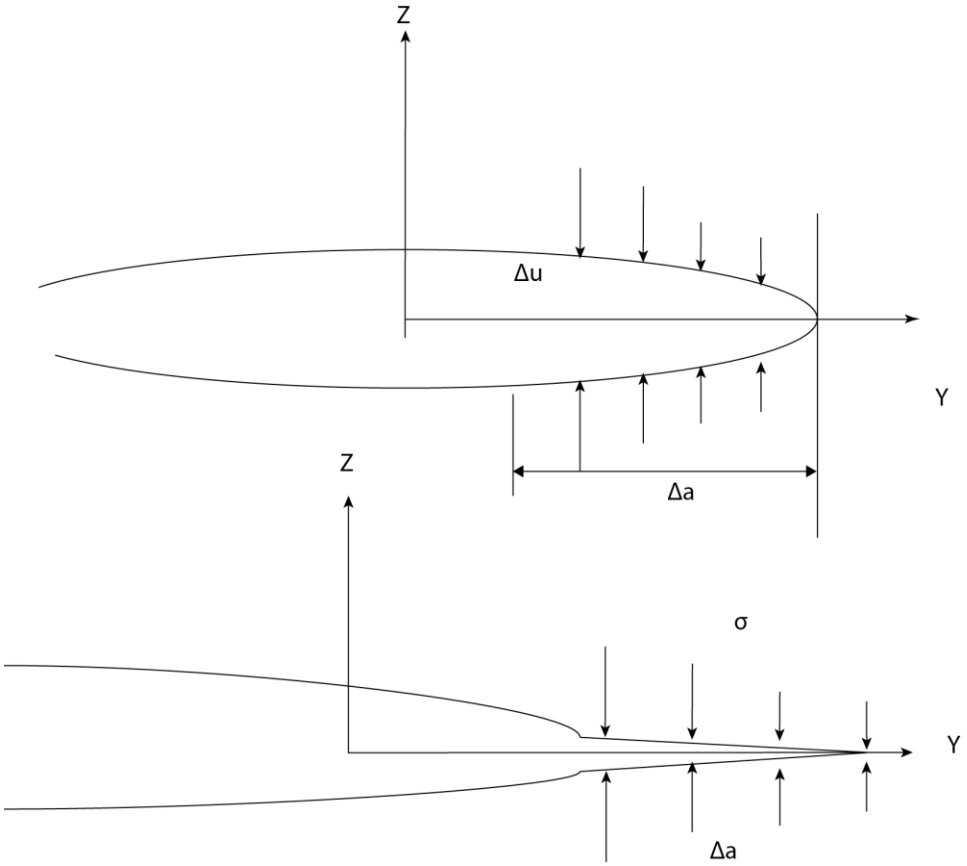

Figure 3-3 Schematic of Crack Closure Technique

According to the Virtual Crack Closure Technique, the evaluation of the Strain Energy Release Rate can be obtained starting from the assumption that for an infinitesimal crack opening, the strain energy released is equal to the amount of the work required to close the crack.

Irwin's crack closure integral can be expressed as,

$$G_I = \lim_{\Delta a \to 0} \frac{1}{2\Delta a} \int_0^a \sigma . \Delta u \, da \tag{3.1}$$

where Δu is a displacement vector between the crack faces, and σ is a vector defining the stress components per unit crack area which are required to close the cracks.

The integral form can be expressed as,

$$G = G_I + G_{II} + G_{III}$$

where,

$$G_I = \lim_{\Delta a \to 0} \frac{1}{2\Delta a} \int_0^{\Delta a} \sigma_z . \Delta w da \tag{3.2}$$

$$G_{II} = \lim_{\Delta a \to 0} \frac{1}{2\Delta a} \int_0^{\Delta a} \sigma_y . \Delta v da \tag{3.3}$$

$$G_{III} = \lim_{\Delta a \to 0} \frac{1}{2\Delta a} \int_0^{\Delta a} \tau_{xz} . \Delta v da \tag{3.4}$$

The components G_I, G_{II}, G_{III} are referred to as mode I, mode II and mode III strain energy release rates corresponding to crack opening, sliding and tearing modes respectively.

Ribicki and Kanninen[7] presented a simple method to Irwin's crack closure model. This technique simplifies the method of calculating the strain energy release rates, because knowledge of the singular stresses near the crack tip is not required.

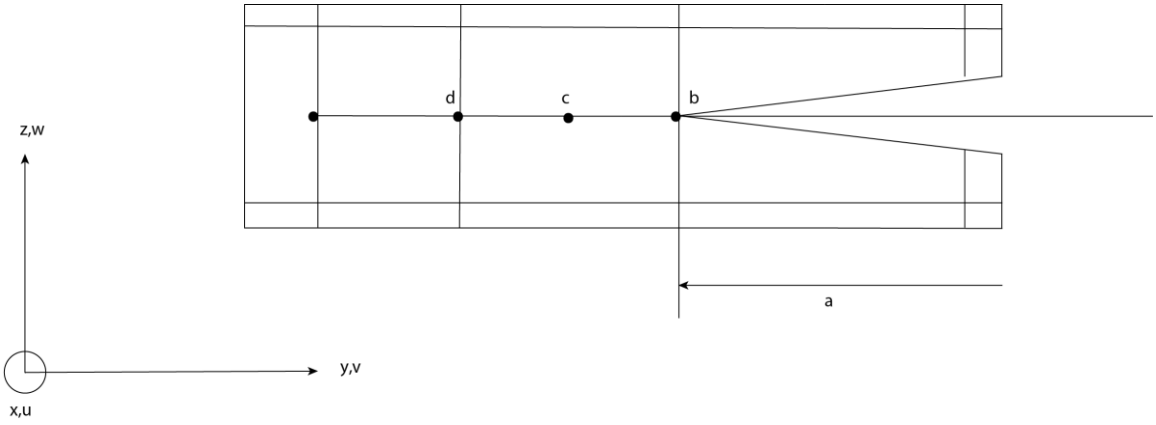

(a) Before Crack Extension

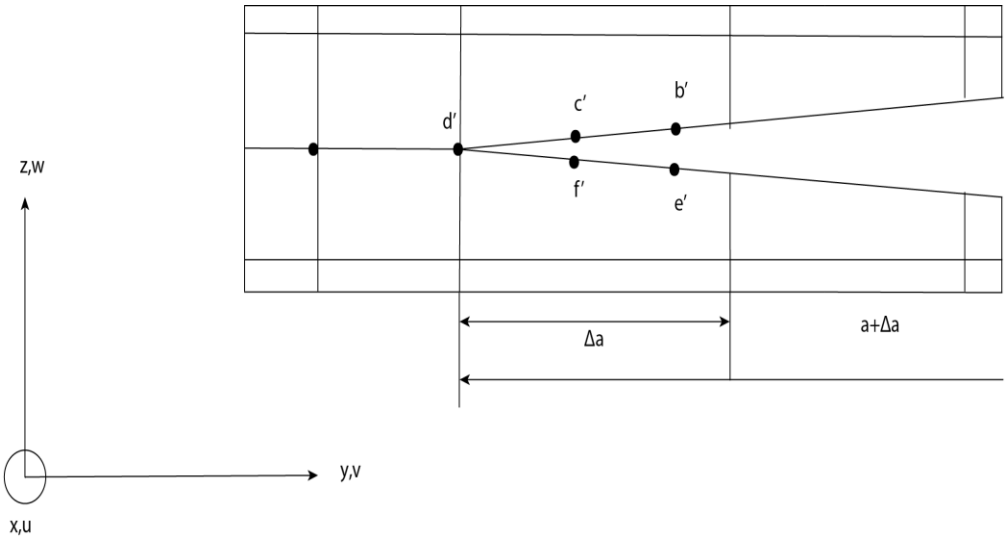

(b) After Crack Extension

Figure 3-4 Crack Closure Technique for Computing Strain Energy Release Rates

The nodal forces are evaluated at the nodes b and c for a crack size a. Then the nodes b and c are released and the crack is allowed to extend an amount of ∆a as shown in fig. After the crack extends, the relative displacements between nodes b' and e', and c' and f' are measured. The energy release rates can now be expressed as the work required to close the crack by an amount ∆a by

$$G_I = \frac{1}{2\Delta a}[F_{zb}(w_{b'} - w_{e'}) + F_{zc}(w_{c'} - w_{f'})] \quad (3.5)$$

$$G_{II} = \frac{1}{2\Delta a}[F_{yb}(v_{b'} - v_{e'}) + F_{yc}(v_{c'} - v_{f'})] \quad (3.6)$$

$$G_{III} = \frac{1}{2\Delta a}[F_{xb}(u_{b'} - u_{e'}) + F_{xc}(u_{c'} - u_{f'})] \quad (3.7)$$

where, for example, F_{xb} is the nodal force in the X direction at node b.

3.2 Cohesive Zone Modeling (CZM)

This technique is the latest addition to ANSYS™, which involves the modeling with the help of cohesive/interface/contact type of elements. This modeling involves the debonding without any prior definition of crack. The nodes along this region have special properties which closely resembles the real case scenario of a laminated composite.

Modeling with CZM has greater advantages as it predicts the growth and delamination. This technique can be implemented with complex structure, but the problem definition requires the characterization data which is difficult to obtain and even the accurate assessments are tied.

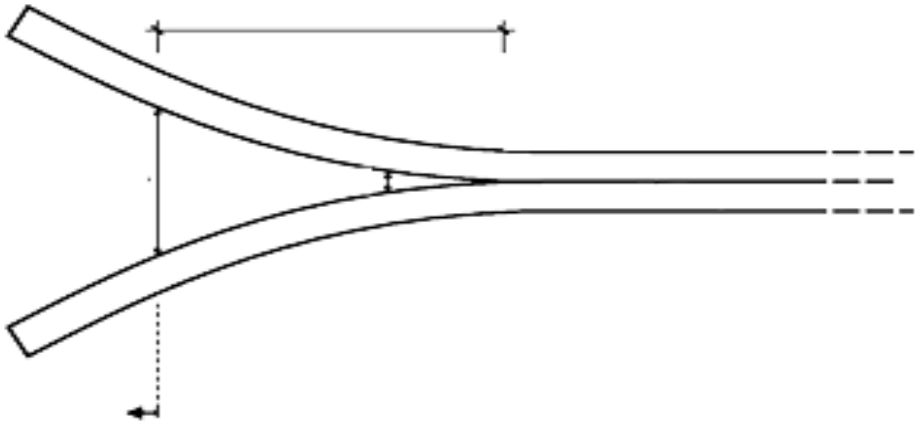

Figure 3-5 Double Cantilever Beam with Cohesive Zone

Element Definition:

An interface element is composed of bottom and top surfaces. The element mid plane can be created by averaging the coordinates of node pairs from the bottoms and top surfaces of the element. The numerical integration of the interface elements is performed in the element mid plane. The Gauss integration scheme is used for the numerical integrations.

Element Selection:

The simulation of an entire assembly, consisting of the cohesive zone and the structural elements on either side of the cohesive zone [8], requires that the interface elements and structural elements have the same characteristics. When you issue the CZMESH command, the appropriate interface element(s) will be selected automatically, depending on the adjacent structural elements. We can also manually specify your interface elements. We actually are modeling cohesive elements with negligible thickness. So, no need to use CZMESH.

Table 3-1 Interface and Structural Elements

For elements with these characteristics:	Interface element:	with one of these structural elements:
2-D, linear	INTER202	PLANE182
2-D, quadratic	INTER203	PLANE183
3-D, quadratic	INTER204	SOLID186, SOLID187
3-D, linear	INTER205	SOLID65, SOLID185**, SOLSH190, SOLID272, SOLID273, SOLID285

Proper element type is chosen based on the stress states of interest and structural element types used.

Material Characteristics:

The CZM option of the TB command lets you define interface separation behavior with ANSYS interface elements. The interface is represented by a single element set of these elements. The interface deformation is characterized by a traction separation law, with the deformation occurring only within the interface elements i.e the cohesive zone. The tension or shear deformations within this zone are of primary interest. The surface behavior of the material is highly nonlinear in either case, and the resulting softening or loss of stiffness changes character rapidly as the element separation increases

Material Constants:

The cohesive zone model (TB, CZM) uses a traction separation law defined as:

$$T_n = e\sigma_{\max}\Delta_n e^{-\Delta_n} e^{-\Delta_t^2} \tag{3.8}$$

For normal traction at the interface, and

$$T_n = 2e\sigma_{\max}\frac{\overline{\delta_n}}{\delta_t}\Delta_t(1+\Delta_n)e^{-\Delta_n}e^{-\Delta_t^2} \tag{3.9}$$

For shear traction at the interface, where:

$$T = \frac{\partial\phi(\delta)}{\partial\delta} \tag{3.10}$$

Modeling the complex composite beam with delamination require conscientious study of these two techniques and implement them in an appropriate manner.

Finally, VCCT has been chosen for this study as this would involve only the assumptions of a crack length, crack growth and loading conditions without presuming any characterized data of a composite beam. The method to calculate the energy release rate using virtual crack extension method is as described earlier.

3.3 Specimen Description

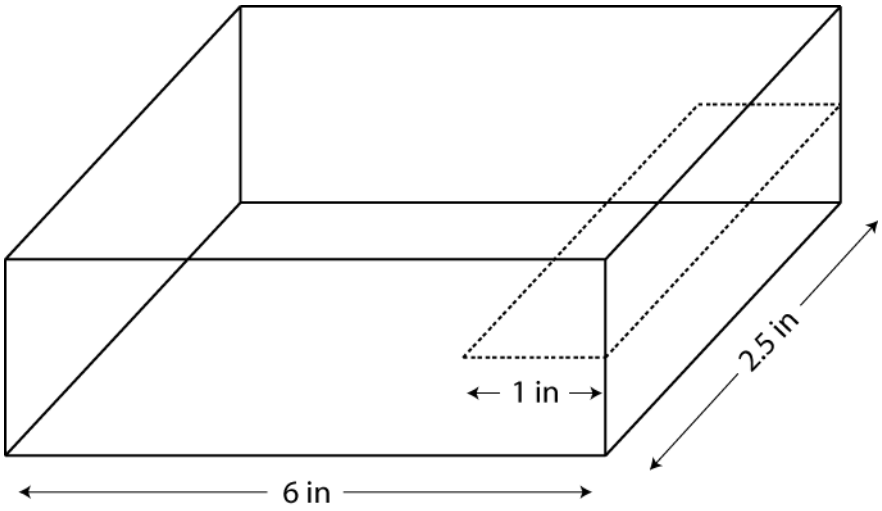

Figure 3-6 Model Description

To perform the analysis in Ansys an apt model is needed to adapt to its environment in order to obtain the solution without any absurdities. This involves a careful evaluation of specimen before performing the analysis. In the present work we assume a model that is suitable to produce results that are in closed form. A specimen of 6 inch length with an initial crack of 1 inch and the thickness of each ply is 0.005 inch is assumed. For a 2-D case the total height will be number of plies times the thickness of each ply. For a 3-D case the width is assumed to be 2.5 inch. These assumptions are made in order to obtain the aspect ratio right and can be varied accordingly.

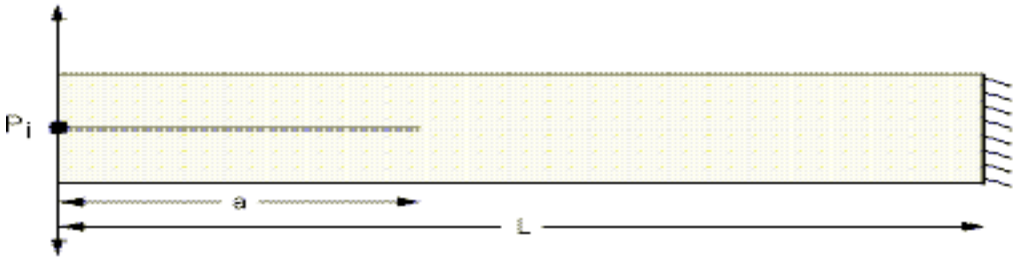

Figure 3-7 Illustration of Double Cantilever Beam

3.4 Specimen Properties

The double cantilever beam specimen has the following properties: (Appendix A)

E_{11}= 161GPa (2.335e7 psi) v_{12}= 0.32 G_{12}= 5.17Gpa (0.74e6 psi)

E_{12}= 11.38GPa (1.65e6 psi) v_{23}= 0.45 G_{23}= 3.92GPa (0.56e6 psi)

E_{13}= 11.38GPa (1.65e6 psi) v_{13}= 0.32 G_{13}= 5.17GPa (0.74e6 psi)

Thermal Properties: (Appendix A)

α_1= -0.0719e-6/^0C α_2=21.2e-6/^0C α_{12}=0

Reference Temperature = 0

Element type selection is based on the type of specimen, applied loads, type of boundary conditions and the displacements of the specimen. In order to acquire an accurate solution an element should satisfy conditions given above. For a 2-D analysis PLANE 182 or SHELL 181 can be used as this analysis is based on orthotropic behavior and the displacements are linear. The nonlinearities in displacements and cracks as well are neglected.

3.4.1 Element Type

PLANE182: It is used for 2-D modeling of solid structures. The element can be used either as a plane element (plane stress or plane strain) or as an axisymmetric element. The element is defined by four nodes having two degrees of freedom at each node.

- Translations in the nodal x and y directions.

- The element has plasticity, stress stiffening, large deflection, and large strain capabilities.

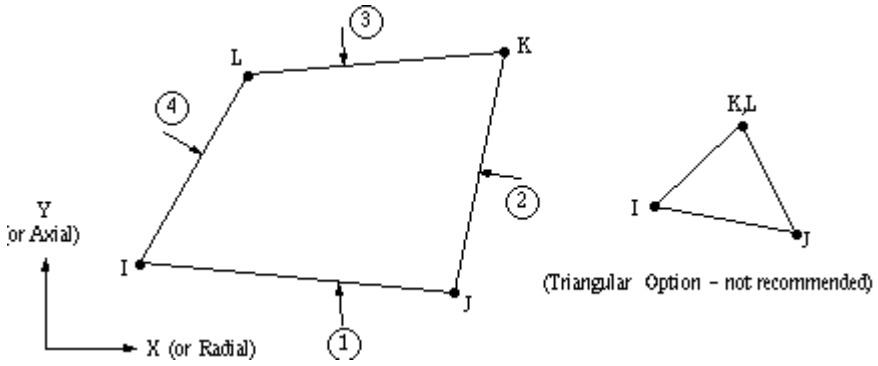

Figure 3-8 PLANE 182 Element Type

SHELL181: It is suitable for analyzing thin to moderately-thick shell structures. It is a four-node element with six degrees of freedom at each node: translations in the x, y, and z directions, and rotations about the x, y, and z-axes. (If the membrane option is used, the element has translational degrees of freedom only). The degenerate triangular option should only be used as filler elements in mesh generation.

SHELL181 is well-suited for linear, large rotation, and/or large strain nonlinear applications. Change in shell thickness is accounted for in nonlinear analyses. In the element domain, both full and reduced integration schemes are supported. SHELL181 accounts for follower (load stiffness) effects of distributed pressures.

SHELL181 may be used for layered applications for modeling composite shells or sandwich construction. The accuracy in modeling composite shells is governed by the first-order shear-deformation theory (usually referred to as Mindlin-Reissner shell theory).

The element formulation is based on logarithmic strain and true stress measures. The element kinematics allow for finite membrane strains (stretching). However, the curvature changes within a time increment are assumed to be small.

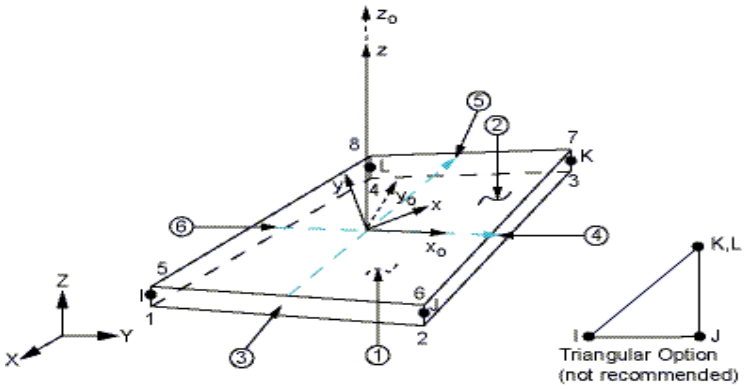

Figure 3-9 SHELL 181 Element Type

3.4.2 Meshing

The specimen is meshed with PLANE 182 elements with the orthotropic properties. The lines are attributed with the aspect ratio matching the thickness in the Y direction and the lines along the length are attributes with an element division based on the focus of study. The crack tip region is meshed coarsely to refine the values obtained near the tip for accuracy. Too fine mesh can be tedious as the study is focused on the separation of nodes. The number of nodes generated is kept optimum for the research with 5124 nodes (3-D) and 244 (2-D).

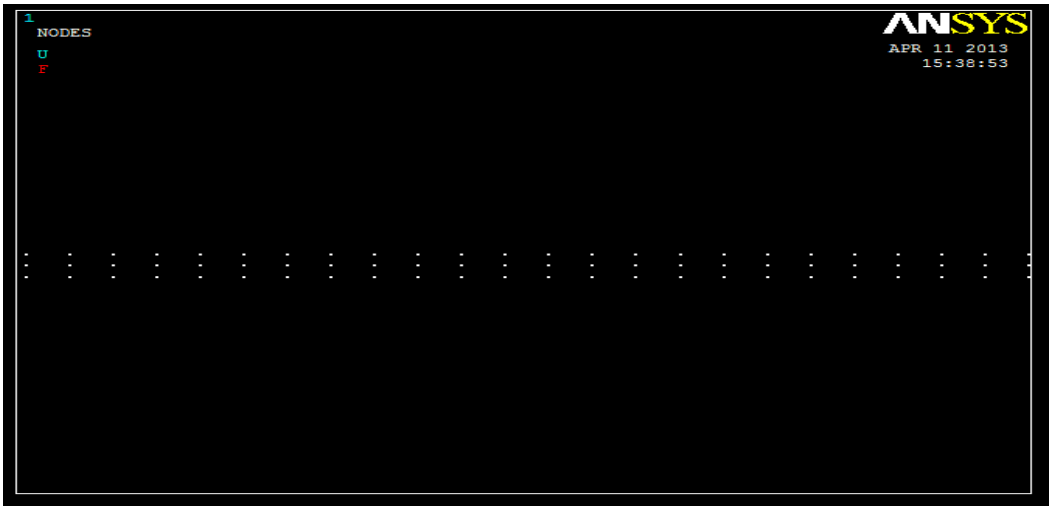

Figure 3-10 2-D Beam Nodes

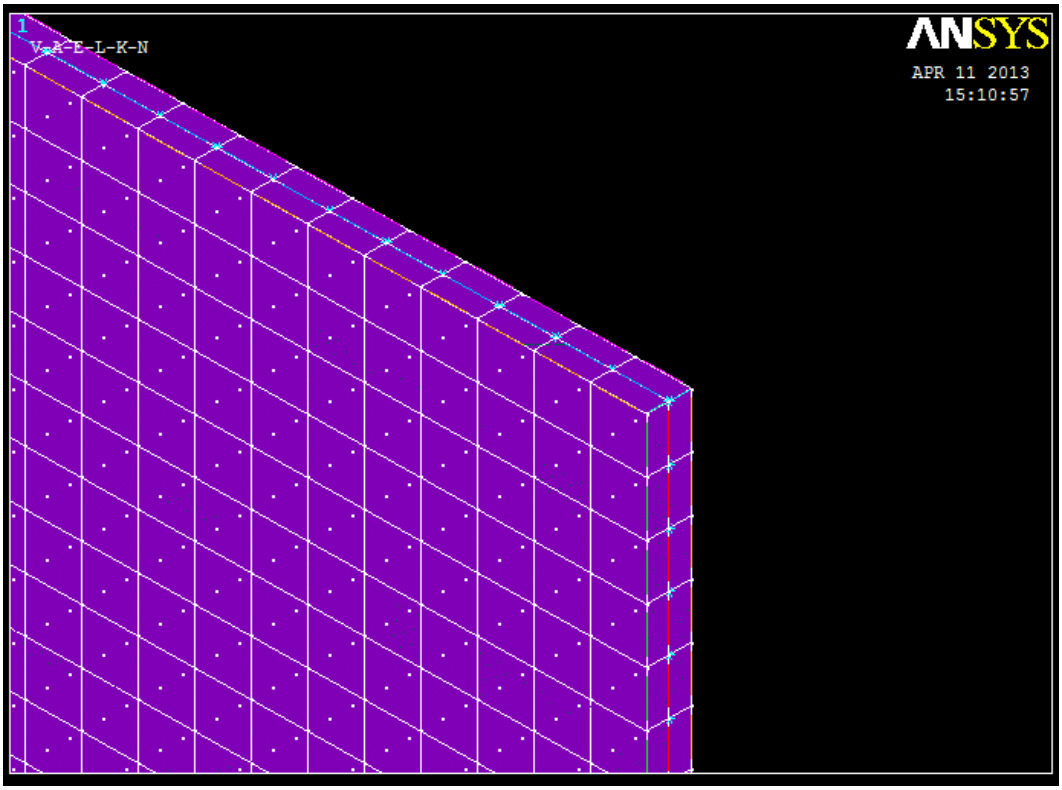

Figure 3-11 3-D Meshed Beam

A 3-D model is meshed using a SOLID 185 element which is capable of modeling a composite structure up to 250 layers. While meshing the areas the aspect ratio is maintained in order to obtain the results accurately. Theoretically the thickness direction should contain a minimum of three nodes defining the surface and the number of nodes in the length and width (3-D) can be any arbitrary value. The meshing can be coarse at the junction where the crack tip is present and the region around the tip. The rest of the specimen is not the subject of interest so the mesh can be fine enough for the solution to converge [9].

Typically this debonding technique is implemented using a contact and target elements at the interface along with Virtual Crack Closure Technique. The contact procedure is a tedious job in the whole analysis as it involves selection of contact nodes (surface in surface to surface contact analysis) and target nodes (surface in surface to surface contact analysis).

A contact is established when two surfaces touch each other such that they become mutually tangent. In the physical sense, surfaces that are in contact have the following characteristics:

- No interpenetration
- Able to transfer the compressive normal forces and tangential frictional forces.
- Do not transmit tensile normal forces.

As a result, they are free to separate and can deviate away from each other. This property in contact analysis is used to develop a delamination model in Ansys. This analysis is usually a nonlinear analysis and the stiffness of the system depends on the contact properties at the parts that are touching or separated. Physically, the bodies are not penetrating so the program must enable a relationship between the surfaces to prevent them from passing through each other in the analysis. So, contact compatibility is enforced by the program to prevent interpenetration and Ansys™ offers several different contact formulations to implement the compatibility at the interface.

For a nonlinear contact analysis we assume Pure Penalty or Augmented Lagrange formulations and these penalty based contact formulations assume,

$$F_{normal} = k_{normal}. x_{penetration} \qquad \text{Pure Penalty} \qquad (3.11)$$

$$F_{normal} = k_{normal}. x_{penetration} + \lambda \qquad \text{Augmented Lagrange} \qquad (3.12)$$

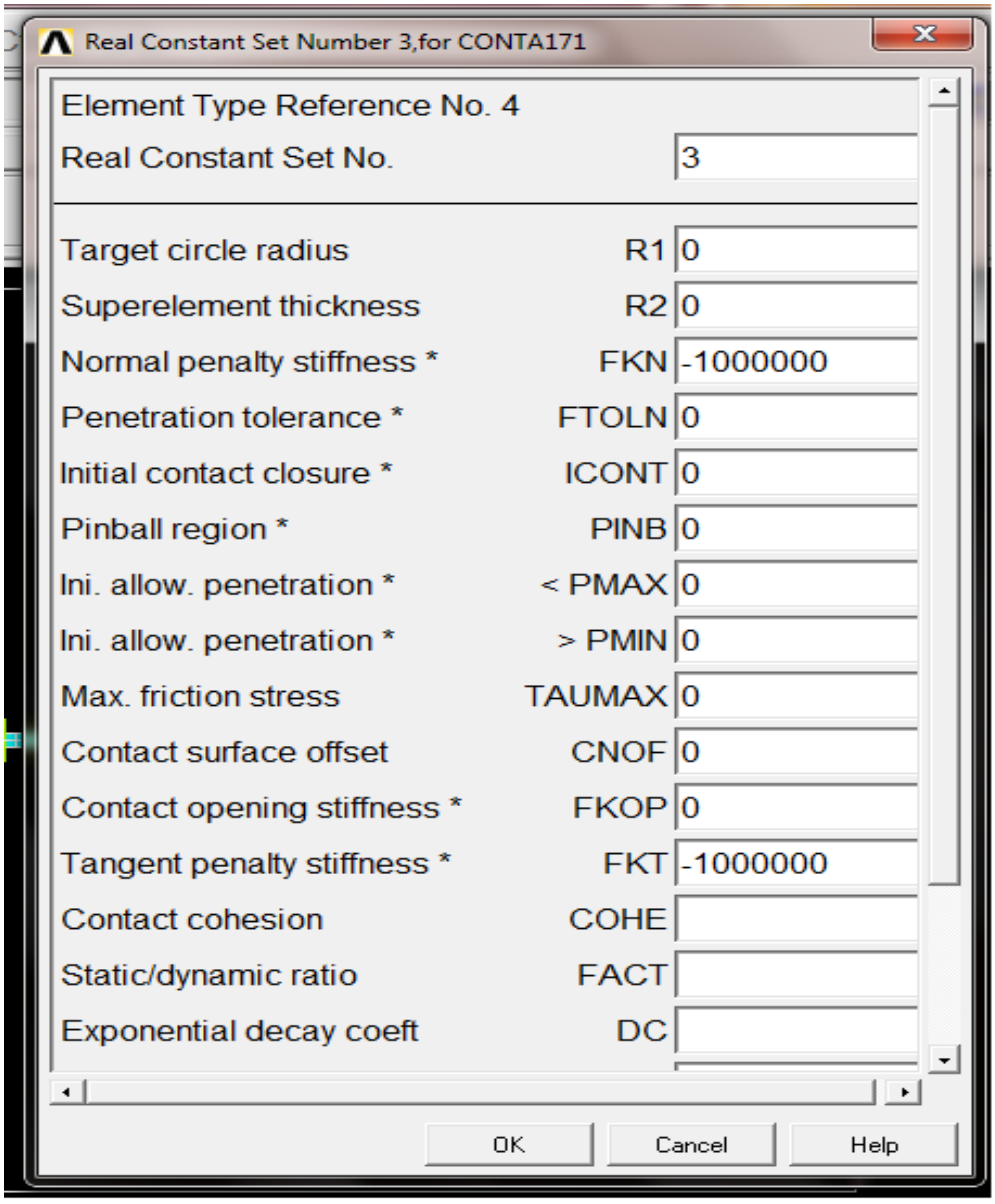

Figure 3-12 Real Constants for Contact Type

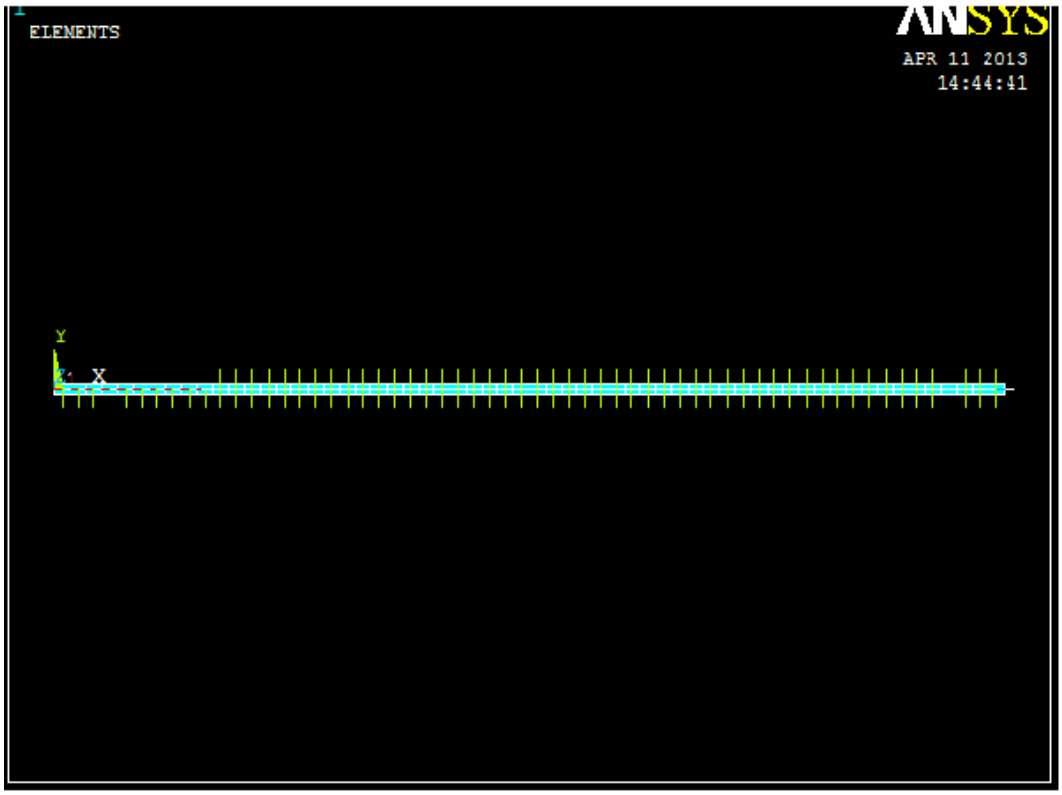

Figure 3-13 Contact and Target Element Normal's

The convergence of solution depends on the contact properties as they have chattering effect. This is predominantly because whenever the contact properties are defined with no penetration the program assumes a Normal Lagrange method which predicts the contact status as either open or closed (a step function) and the convergence may oscillate between open or closed status called chattering. If some penetration is allowed it makes the convergence easier since the contact is no longer a step function.

Contact analysis needs the properties to be defined along the interface and these are different from the regularly defined material properties which are specimen properties. A special function called "TBDATA" enables to define the new properties along the interface. For this kind of analysis the interfacial properties are defined based on the assumptions and some experimental data to obtain a strain energy release rate for the delamination.

Boundary conditions and Loading:

The specimen represents a double cantilevered beam so one end of the beam is fixed with no degrees of freedom i.e

$U_x = 0$ $U_y = 0$ $U_z = 0$

ROTX = 0 ROTY = 0 ROTZ = 0 (3-D)

$U_x = 0$ $U_y = 0$

ROTX = 0 ROTY = 0 (2-D)

The free end is subjected to a load which can be either in the form of displacement or in the form of direct load. In case of thermal loading a uniform temperature load is applied.

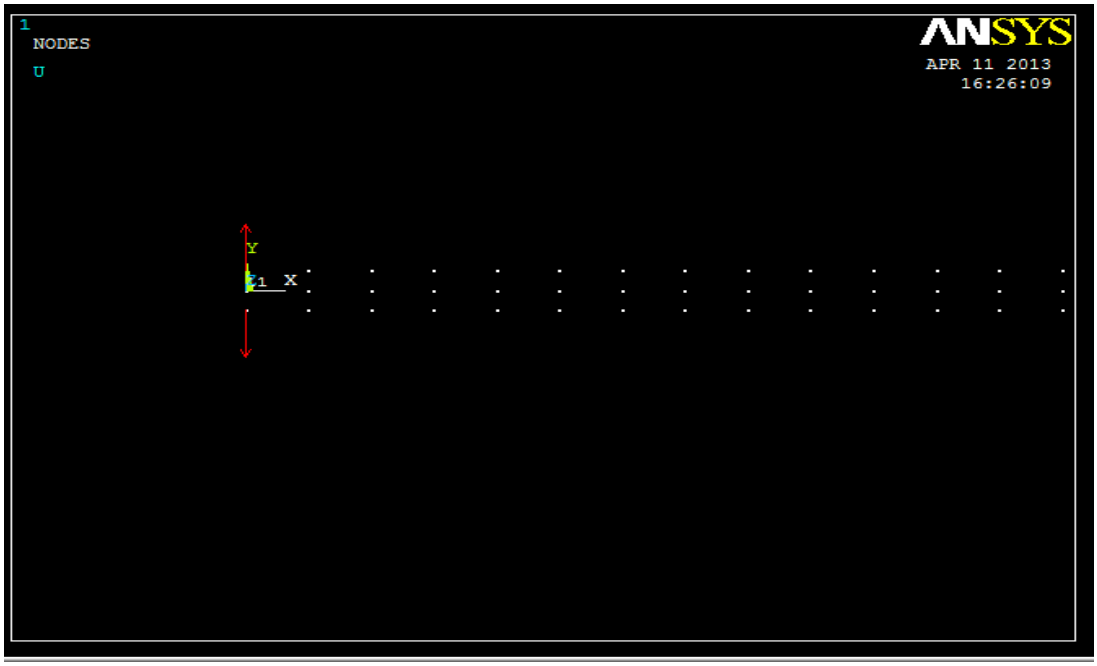

Figure 3-14 Loads (Force) Applied on Nodes

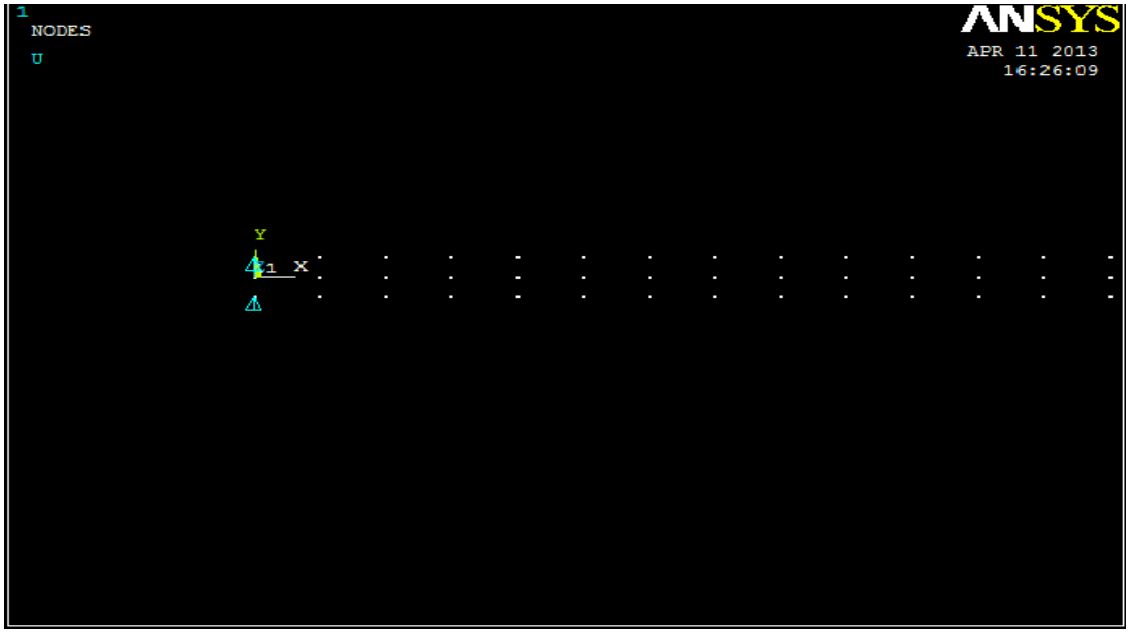

Figure 3-15 Loads (Displacement) Applied on Nodes

The loads will be based on the assumption of the available strain energy release rate in order to obtain the convergence. The closed form convergent solution for the current problem is given by Fig 3-12.

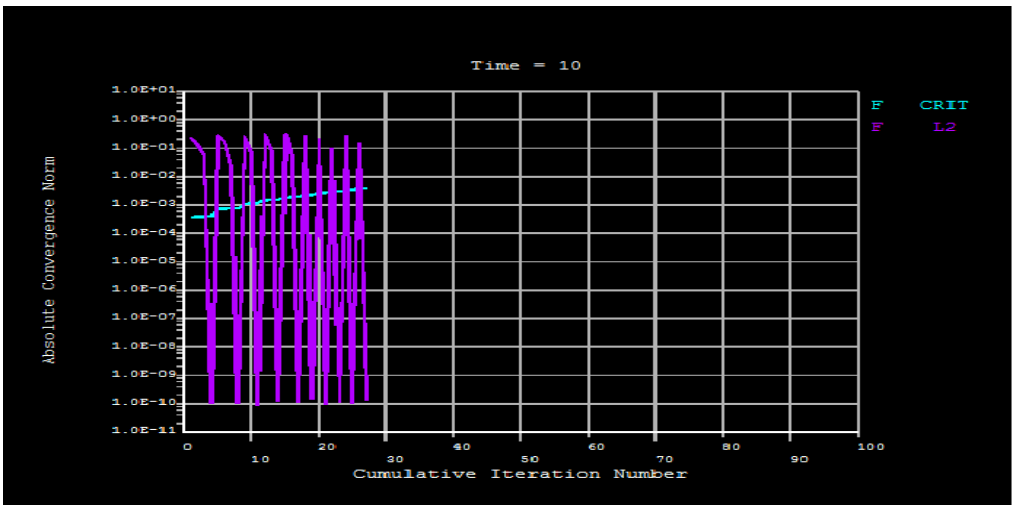

Figure 3-16 Solution Convergence

The time step defined for this nonlinear analysis is in the order of 10 which is only for the case of simplicity and the convergence can be obtained with a lesser time step also. This can be achieved by reducing the substeps to a value closure to 1.

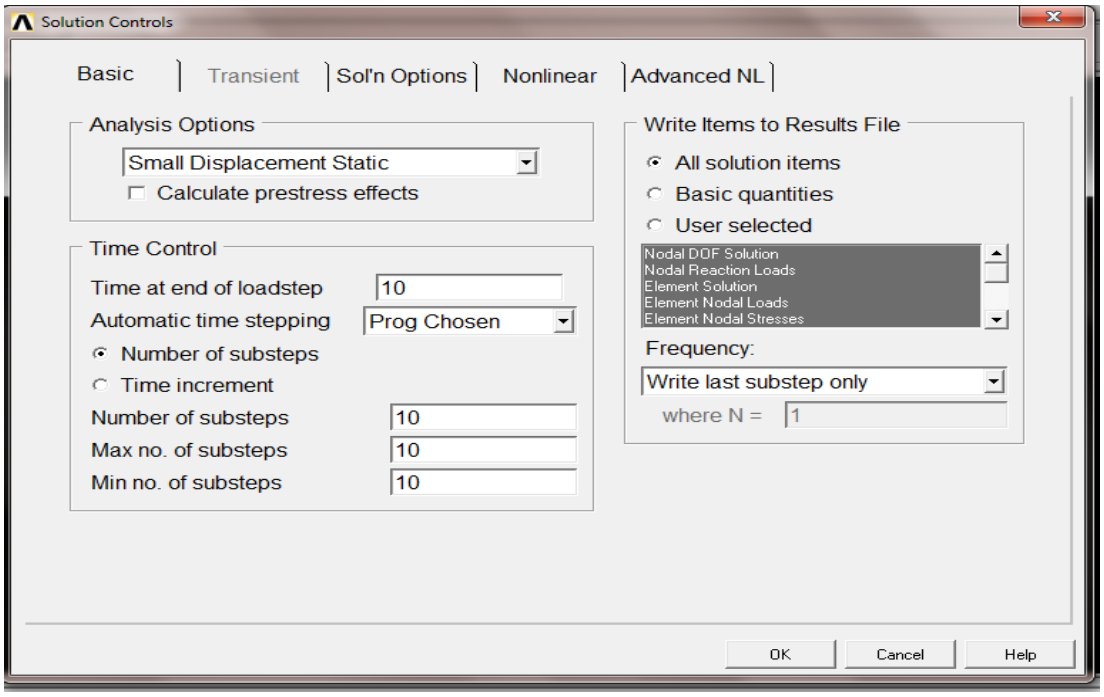

Figure 3-17 Time Step Increment Illustration

Chapter 4

Parametric Study and Discussion

In this chapter, we first to compare the results of the strain energy release rate obtained by the present analytical and finite element methods. With validation of analytical method, we conduct the parametric study on the variation of strain energy release rate due to temperature change, percentage of 90 plies in the laminate of $[0_n/90_m]_s$, percentage of $\pm 45^o$ plies in the laminate of $[0_n/\pm 45_m]_s$. Although the delamination occurring at the mid-plane of the laminate, $[0_n/\pm 45_m]_s$, the fracture mode is not just a pure Mode I fracture. It is a combination of Mode I, II and III. This is because of all of the shear stresses present at the interface. These shear stresses contribute to the delamination growth. A study to investigate the contribution of Mode II and Mode III is also conducted. Finally, a study of effect of strain energy release rate due to unsymmetry is also investigated.

4.1 Validation of Present Model and FEM for Calculating Strain Energy Release Rate

The laminate considered here is $[0_{16}]_S$. The strain energy release rate values obtained from the Finite element analysis using VCCT in Ansys for pure mechanical loading and with thermal loading respectively for a ply stacking sequence of $[0_{16}]_S$ are presented below. Figure 4.1 and 4.2 shows the strain energy release rate variation obtained by FEM and the present analytical method, respectively. The strain energy release rate is normalized by the applied load, P. The numerical values of strain energy release rate are tabulated in Table 4.1 with percentage difference between these two methods. Figures 4.1 and 4.2 show that the effects of temperature on strain energy release rates are insignificant.

As indicated in Table 4.1, the results obtained from the present method agree well with the results obtained by FEM.

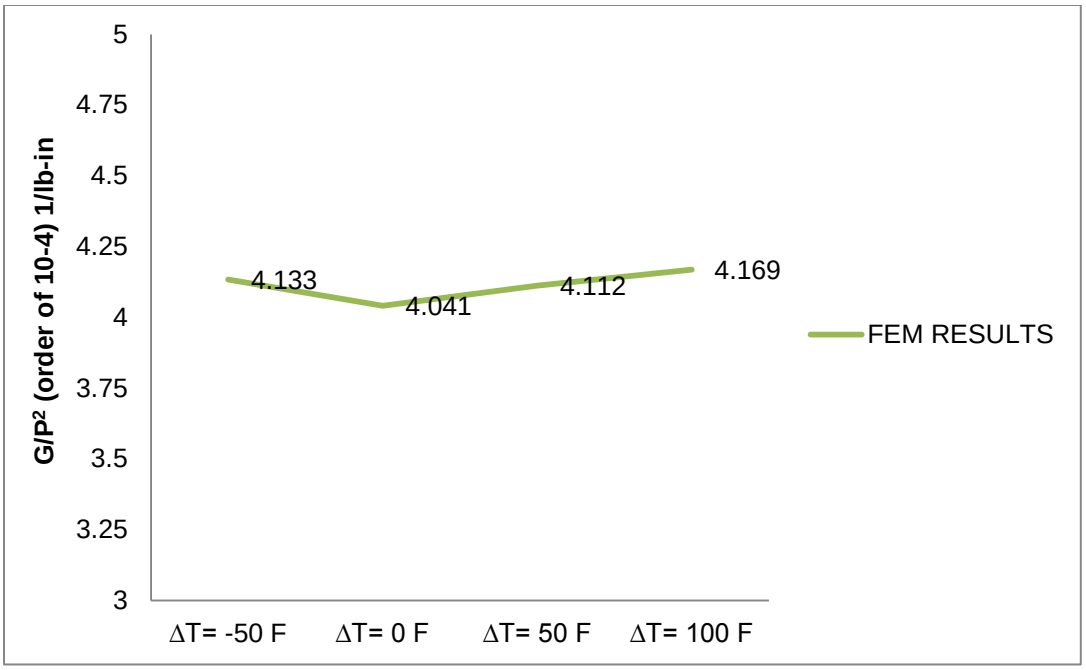

Figure 4-1 Variation in SERR FEM analysis

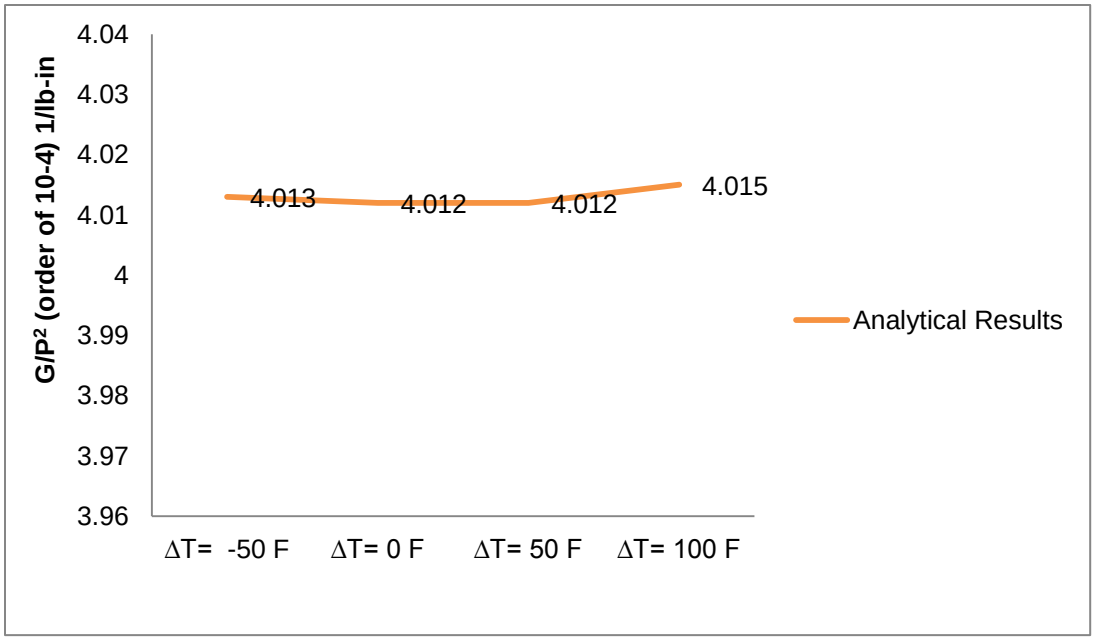

Figure 4-2 Variation in SERR Analytical results

Table 4.1 Comparison of Strain Energy Release Rate by Present and FEM Methods

SPECIMEN/ MATERIAL	LOADING CONDITION	FEM RESULT G/P^2(1/lb-in)(10^{-4})	ANALYTICAL G/P^2(1/lb-in) (10^{-4})	% ERROR
DCB/IM7 8552	P+(ΔT=-50F)	4.133	4.013	2.4
DCB/IM7 8552	P+(ΔT=0F)	4.041	4.012	0.69
DCB/IM7 8552	P+(ΔT=50F)	4.112	4.012	2.3
DCB/IM7 8552	P+(ΔT=100F)	4.169	4.015	3.7

4.2 Variation of Strain Energy Release Rate with Percentage of 90^0 Plies in [0/90]s Laminate

Table 4.2 list the normalized strain energy release rate for IM7/8552 laminate with various percentage of $[0_n/90_m]_s$ layups.

Table 4.2 Normalized Strain Energy Release Rate with % 90 plies in $[0_n/90_m]_s$ Present and FEM Methods

Specimen Type	Material Type	Stacking Sequence	G/P^2 P+(ΔT=0F) (1/lb-in) (10^{-4})	G/P^2 P+(ΔT=50F) (1/lb-in) (10^{-4})	G/P^2 P+(ΔT=100F) (1/lb-in) (10^{-4})
DCB	IM7/8552	$[0]_{16S}$	4.041	4.112	4.169
DCB	IM7/8552	$[0/90_{14}/0]_S$	10.58	10.95	11.99
DCB	IM7/8552	$[0_2/90_{12}/0_2]_S$	6.568	6.772	7.353
DCB	IM7/8552	$[0_3/90_{10}/0_3]_S$	5.167	5.309	5.714
DCB	IM7/8552	$[0_4/90_8/0_4]_S$	4.524	4.659	4.941
DCB	IM7/8552	$[0_5/90_6/0_5]_S$	4.210	4.297	4.542
DCB	IM7/8552	$[0_6/90_4/0_6]_S$	4.069	4.142	4.336
DCB	IM7/8552	$[0_7/90_2/0_7]_S$	4.050	4.077	4.237

The data in Table 4.2 is plotted in Figure 4.3 as a variation of percentage of 90 ply in the laminate. Since increasing the percentage of 90 ply in the laminate, the higher thermal strain energy along the longitudinal direction is produced. This trend is shown in Figure 4. 3. It is also shown the thermal effect on strain energy release rate is more pronounced for high percentage of 90^0 ply than lower percentage of 90^0 ply in the laminate. It should be noted that there is a very little shear stresses existing at the tip of delamination. Hence, contribution of mode II and Mode III components to the total strain energy release rate in immaterial. However, this is not the case for $[0_n/\pm 45_m]_s$ laminate.

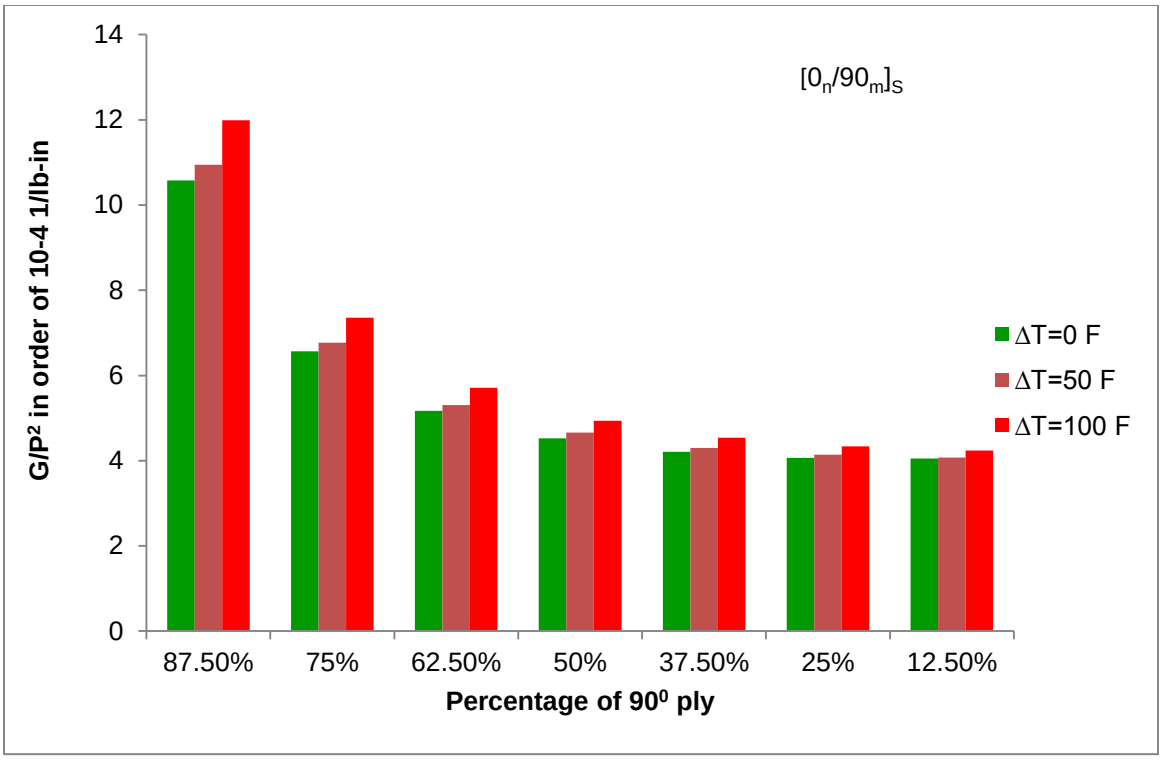

Figure 4-3 Normalized G versus % of 90^0 ply in $[0_n/90_m]_S$ Laminate

4.3 Variation of Strain Energy Release Rate with Percentage of ± 45 Plies in $[0_n/\pm 45_m]_s$ Laminate

Table 4.3 lists the normalized strain energy release rate (G) with various percentage of ± 45 under different temperature environment.

Table 4.3 Normalized G with Various Percentage of ± 45 Plies in $[0_n/\pm 45_m]_s$ Laminate

Specimen Type	Material Type	Stacking sequence	G/P^2 P+(ΔT=0F) (1/lb-in)10^{-4}	G/P^2 P+(ΔT=50F) (1/lb-in) 10^{-4}	G/P^2 P+(ΔT=100F) (1/lb-in) (10^{-4})
DCB	IM7/8552	$[0_2/\pm 45_3/\mp 45_3/0_2]_S$	7.385	7.389	7.456
DCB	IM7/8552	$[0_4/\pm 45_2/\mp 45_2/0_4]_S$	4.561	4.666	4.889
DCB	IM7/8552	$[0_6/\pm 45/\mp 45/0_6]_S$	4.327	4.387	4.553

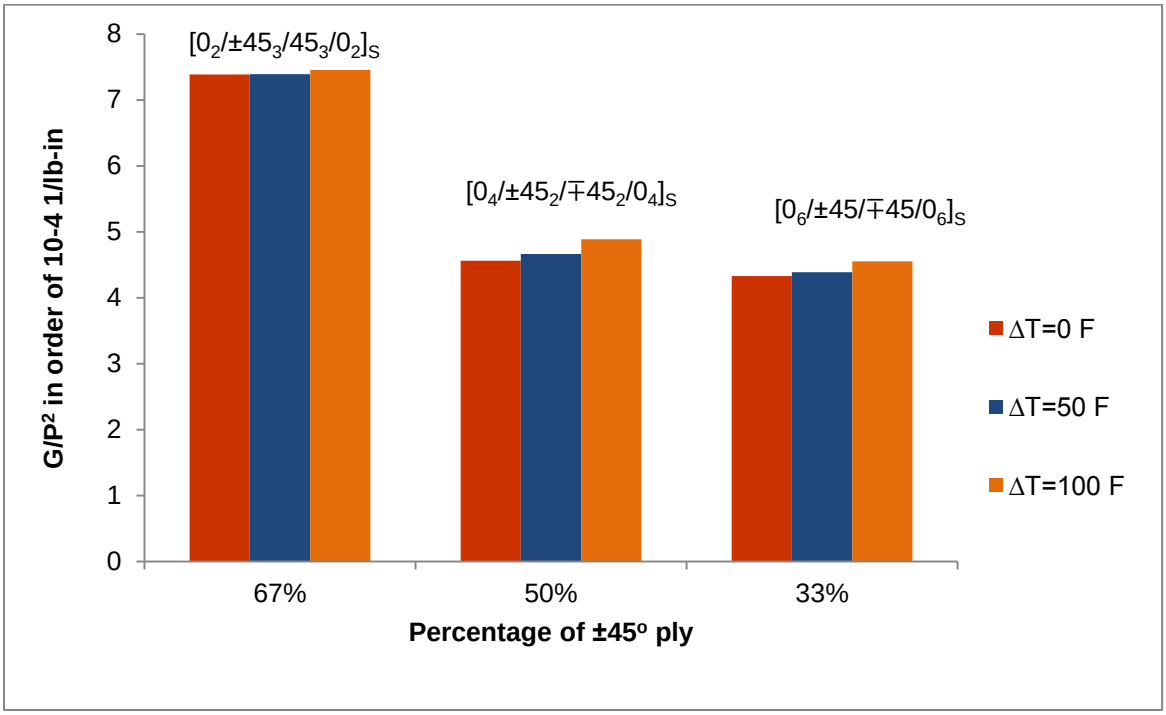

Figure 4.4 Normalized G versus % of $\pm 45^0$ ply in $[0_n/\pm 45_m]_S$ Laminate

4.4 Mode II and III components of Strain Energy Release Rate with Different Temperature Environment

Since, the strain energy values are not purely mode I we need evaluate the percentage of Mode II and Mode III in the stacking sequence. This is given in Table 4.4. As indicated in the

table, the maximum % of G_{II} and G_{III} to G_total ratio is less than 5%. For $[0_n/\pm45_m]_s$ laminate, G_{II} is almost null (less than 0.2%), but G_{III} is less than 3% of G total. For $[0_n/90_m]_s$ laminate, G_{III} is less than 0.3 % of G total. The variation of Mode III component among the laminates with different % of ±45 ply is plotted in Figure 4.5. It is shown that decreasing % of ±45 ply in the laminate the strain energy release rate is decreased.

Table 4.4 Variation of G_{II} and G_{III} to total G Ratio with Different Temperature Environment.

Ply Stacking sequence	G/P^2 (1/lb-in) (10^{-4})		$\%G_{II}/G_T$		$\%G_{III}/G_T$	
IM7/8552	ΔT=50F	ΔT=100F	ΔT=50F	ΔT=100F	ΔT=50F	ΔT=100F
$[0_2/\pm45_3/\pm45_3/0_2]_S$	7.537	7.967	0.139	0.152	2.431	2.639
$[0_4/\pm45_2/\pm45_2/0_4]_S$	4.666	4.889	0.101	0.113	1.875	2.098
$[0_6/\pm45/\pm45/0_6]_S$	4.387	4.553	0.760	0.924	1.444	1.586
$[0/90_{14}/0]_S$	10.95	11.99	3.456	4.595	0.211	0.381
$[0_2/90_{12}/0_2]_S$	6.772	7.353	2.652	3.373	0.194	0.332
$[0_3/90_{10}/0_3]_S$	5.309	5.714	1.971	2.227	0.147	0.291

Table 4-4 Continued

$[0_4/90_8/0_4]_S$	4.659	4.941	1.461	1.892	0.122	0.252
$[0_5/90_6/0_5]_S$	4.297	4.542	0.532	0.953	0.089	0.212
$[0_6/90_4/0_6]_S$	4.142	4.336	0.364	0.421	0.076	0.182
$[0_7/90_2/0_7]_S$	4.077	4.237	0.251	0.332	0.063	0.151

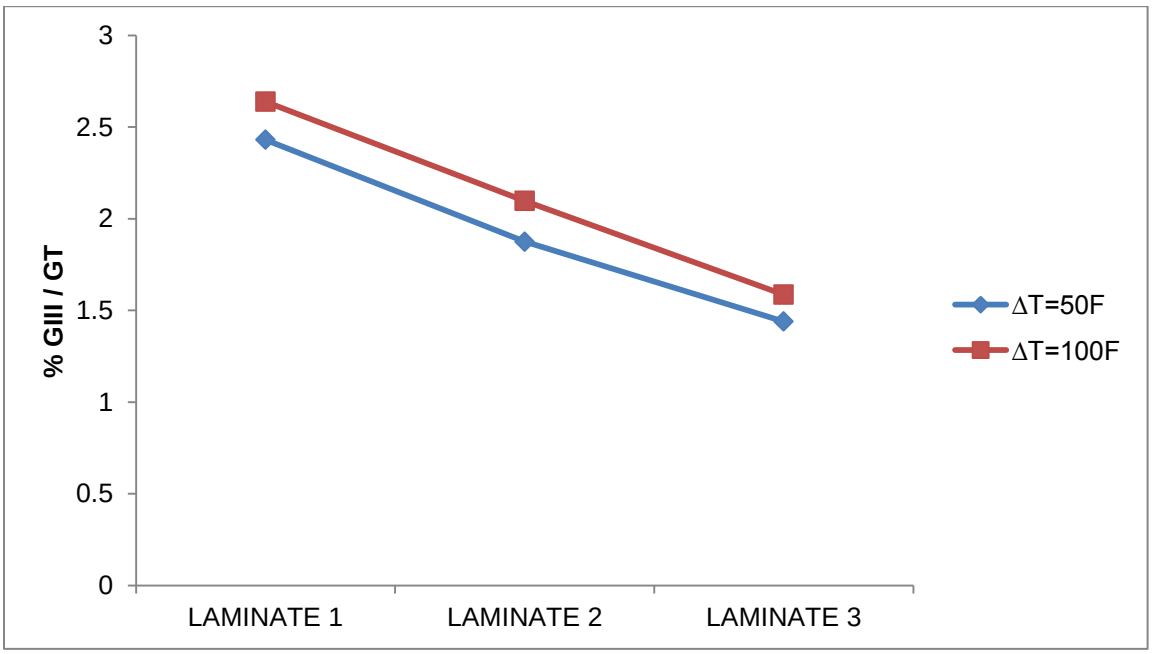

LAMINATE 1: $[0_2/\pm45_3/\mp45_3/0_2]_s$; LAMINATE 2: $[0_4/\pm45_2/\mp45_2/0_4]_s$;
LAMINATE 3: $[0_6/\pm45/\mp45/0_6]_s$

Figure 4.5 Normalized G versus % of ±45 ply in $[0_n/\pm45_m]_S$ Laminate

4.5 Variation of Strain Energy Release Rate of Different Materials in Temperature Environment.

Three different materials were considered, ranging from thermoplastic matrix (AS4/PEEK), toughened matrix (IM7/8552) and brittle matrix composites (T300/5208). The calculated strain energy release rates for these materials are tabulated in Table 4-5. As expected, strain energy release rate is the highest for the composite with thermoplastic matrix material (AS4/PEEK) and the lowest for the composite with the brittle matrix composite (T330/5208). The data is also indicates that increasing temperature, the strain energy release rate is slightly increased for the thermoplastic matrix composite and toughened matrix composite, but decreased for the brittle matrix composite. This is due to the high internal energy in longitudinal direction which results in loss of SERR.

Table 4-5 predicting the strain energy release rate for different materials

Material Type	Laminate Group	Specimen Type	G/P^2 P+(ΔT=0F) (1/lb-in) (10^{-4})	G/P^2 P+(ΔT=50F) (1/lb-in) (10^{-4})	G/P^2 P+(ΔT=100F) (1/lb-in) (10^{-4})
IM7/8552	$[0_{16}]_{2T}$	DCB	4.04	4.11	4.169
T300/5208	$[0_{16}]_{2T}$	DCB	2.8409	2.7043	2.5714
AS4/PEEK	$[0_{16}]_{2T}$	DCB	4.708	4.7772	4.8473

4.6 Comparison of Strain Energy Release Rate between Symmetric and Unsymmetrical Laminates

A comparison of strain energy release rate for laminates with symmetric and unsymmetrical layups is shown in Figure 4.6 through 4.8. It is shown that the laminate with unsymmetrical layup gives higher strain energy release rate comparing with a symmetric layup.

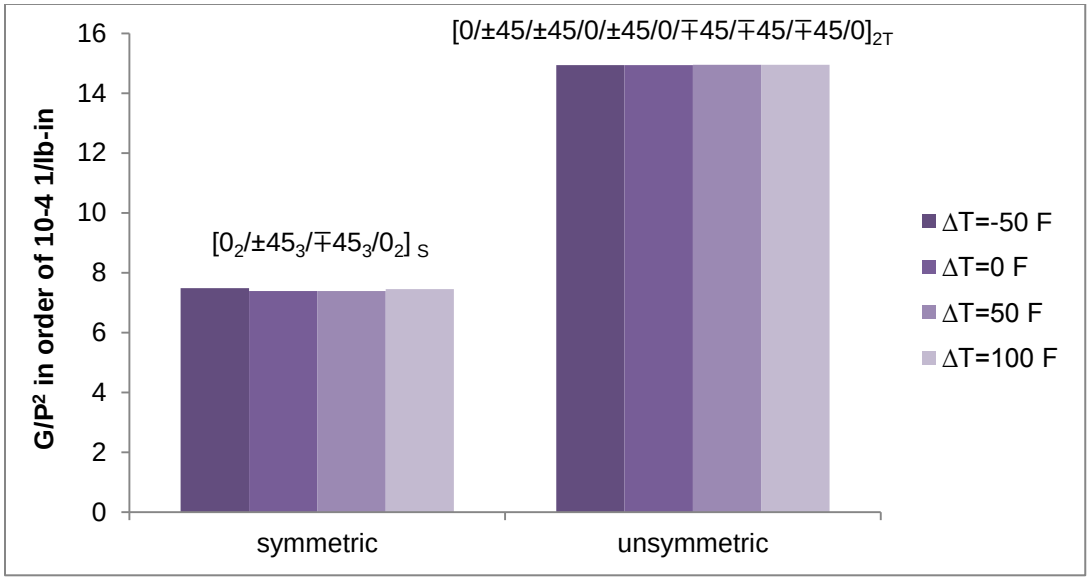

Figure 4.6 Comparison of Normalized G of $[0_n/\pm 45_m]_S$ Laminate with Symmetric and Unsymmetrical Layups in Different Temperature Environment

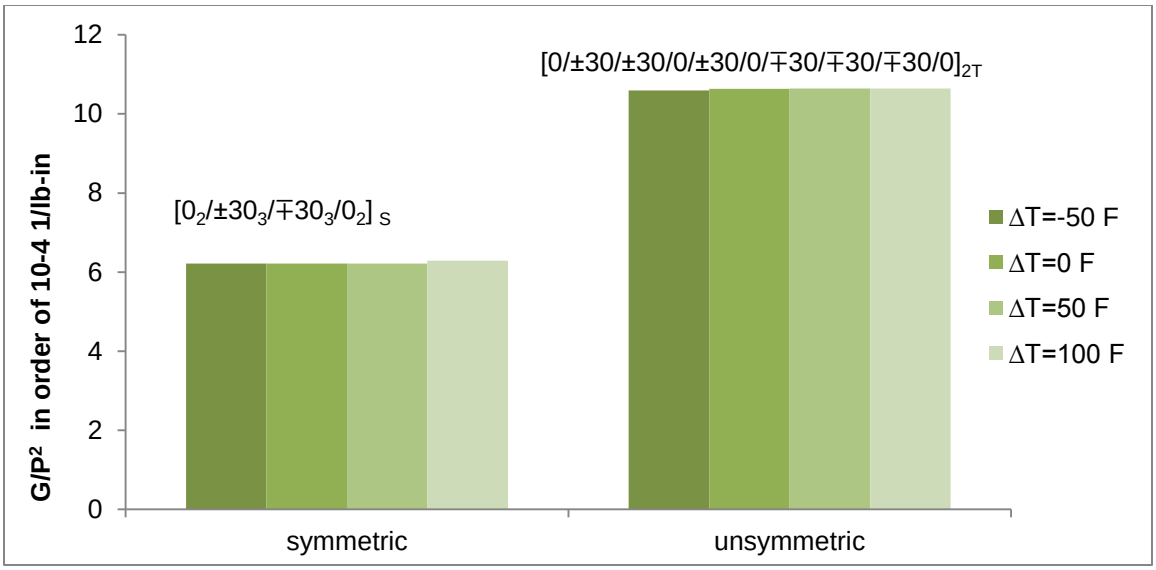

Figure 4.7 Comparison of Normalized G of $[0_n/\pm30_m]_S$ Laminate with Symmetric and Unsymmetrical Layups in Different Temperature Environment

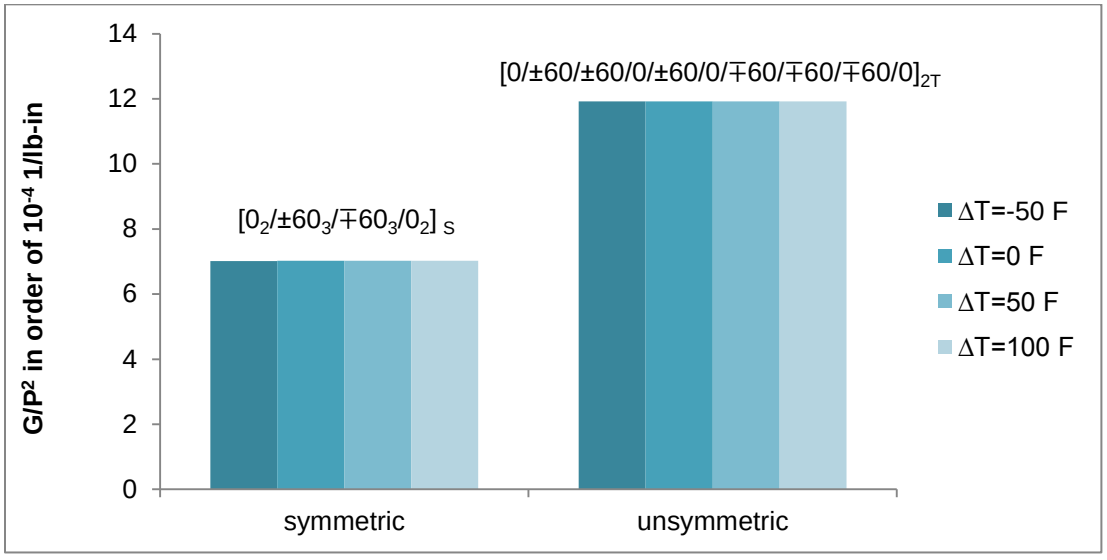

Figure 4.8 Comparison of Normalized G of $[0_n/\pm60_m]_S$ Laminate with Symmetric and Unsymmetrical Layups in Different Temperature Environment

Chapter 5

Results Discussion

Inter laminar fracture tests on IM7/8552 carbon/epoxy results were found to be in correspondence with the expected. The critical strain energy release rate acquired from statistical data is found to be around 1.14 lb/in which is required for the initiation of the crack at the crack front ideally on the specimen described in Figure 3-6. In order to provide the required amount of energy for the crack to propagate termed as available strain energy, the load is increased by 40% of its initial value which produces a strain energy release rate of 1.445 lb/in which is 25% higher than the critical strain energy release rate value. The increase in the value of strain energy release rate (SERR) with the applied load recalls the proportionality relation between G and P.

$$G \propto P^2$$

The change in SERR is satisfactory as the increased load is providing the driving force for the debonding. A similar approach is followed even for the temperature environment. The same specimen is subjected to a temperature loading. An elevation in temperature of $50\,^{O}F$ increased the SERR by 0.21%. This change in value is predicted with the knowledge about thermal forces and moments that are induced when there is an increase in temperature. The variation is significant in terms of SERR as 8552 is a toughened epoxy with excellent mechanical properties and a very good matrix in elevated temperature environment. Based on these conditions, the matrix and carbon fibers will produce shear stresses due to the applied load, leading to delamination and not fiber failure. The matrix 8552 was developed as a controlled flow system, it can be operated in an environment up to $121\,^{O}C$ ($250\,^{O}F$). So, an elevated temperature of $100\,^{O}F$ produce a strain energy release rate of 1.500 lb/in which is higher than the pure mechanical loading case. It is clearly evident that, when a specimen is subjected to temperature environment the SERR will be experiencing additional loads in the form of thermal

forces and moments which are impossible to suppress as in the case of mechanical forces and moments. This provides a strong indication that an elevated temperature will have unquestionable effect on SERR. On contrary, SERR is the basic criterion for the measure of crack initiation, growth and stability. The mechanics of crack is also affected significantly as SERR provides the driving force for the crack propagation. So, an increased value of SERR will lead to crack growth and may finally lead to higher delaminated region. This entire discussion is based only on Finite element results from ANSYS.

The analytical derivation presented in chapter 2 and the results tabulated in table 4.2 will justify the discussion on effects of elevated temperatures on SERR and predicts the variation significantly in case of high change in temperature from reference temperature (usually zero/ room temperature). The analytical formulation predicts the value of SERR on the same specimen described in Chapter 2 as 1.444 lb/in. This value exceeds the critical strain energy since the crack has acquired the driving force to propagate, initiating the growth and delamination as well. When the specimen is subjected to a temperature variation of $50\,^{o}F$ the value of SERR is increased by 2.5% and for a temperature elevation of 100 ^{o}F the change is even more significant and it is 9.3% higher. This clearly establishes the proportionality cited formerly.

When the differences between Fem result and Analytical results were analyzed the SERR appears to be close enough supporting the analytical formulations. The FEM requires some characterized data for enhanced accuracy in ANSYS. The percentage error is less in all different cases. As the results in both cases complementing each other, the research was oriented to instigate the similar accuracy from the analytical formulations with different stacking sequences by integrating with percentage of $\pm 45^{o}$ and 90^{0} plies. This will provide a broader way to understand the delamination in temperature environment. The SERR predicted by ANSYS for 67%, 50%, and 33% of $\pm 45^{o}$ plies shows the compliance with the expected values. The value of

SERR appears higher than $[0]_{16S}$ laminate. Since the integration of $\pm 45^{O}$ will make the laminate soft and this would increase the SERR. Also, as $\pm 45^{O}$ has Mode III domination the value of G_T will definitely be higher. Greater the percentage of $\pm 45^{O}$ plies the higher will the value of SERR. Accordingly, Table 4.3 clearly indicates the value for 75% of $\pm 45^{O}$ is higher than 67% and 33% of $\pm 45^{O}$. This value gradually falls down as the percentage of $\pm 45^{O}$ is decreased and simultaneously increasing the percentage of 0^0 plies.

Correspondingly, the next study is based on 90^0 plies. When 90^0 plies are incorporated then the laminate becomes even softer and the SERR escalations. This is exactly predicted by ANSYS. Typically, the value of SERR falls down with the rise in percentage of 0^0 plies depicting the trend for $\pm 45^{O}$ and 90^0. It is in accordance with the expected values. This can attributed to the Mode II domination in $90°$ laminate.

Hardly understanding the SERR will not suffice the whole concept as the prediction involves the contribution from G_{II} and G_{III} which will have a greater impact on the G_T. So a thoughtful study will assist in clearly understanding the underlying effects and actual reasons for the variation. In table 4.4 the variation in Mode II and Mode III is clearly predicted by FEM approach. The discussion is elaborated by changing the material from IM7/8552 to AS4/PEEK and T300/5208. These values are closely accurate to the expected values.

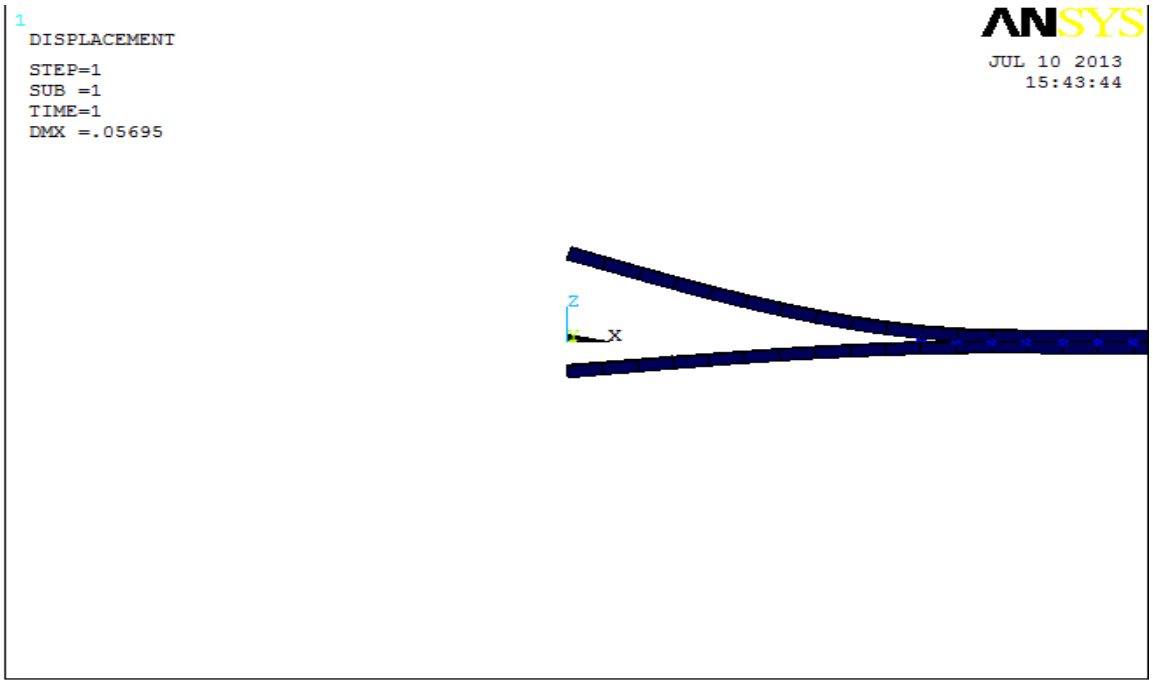

Figure 5.1 Crack Tip

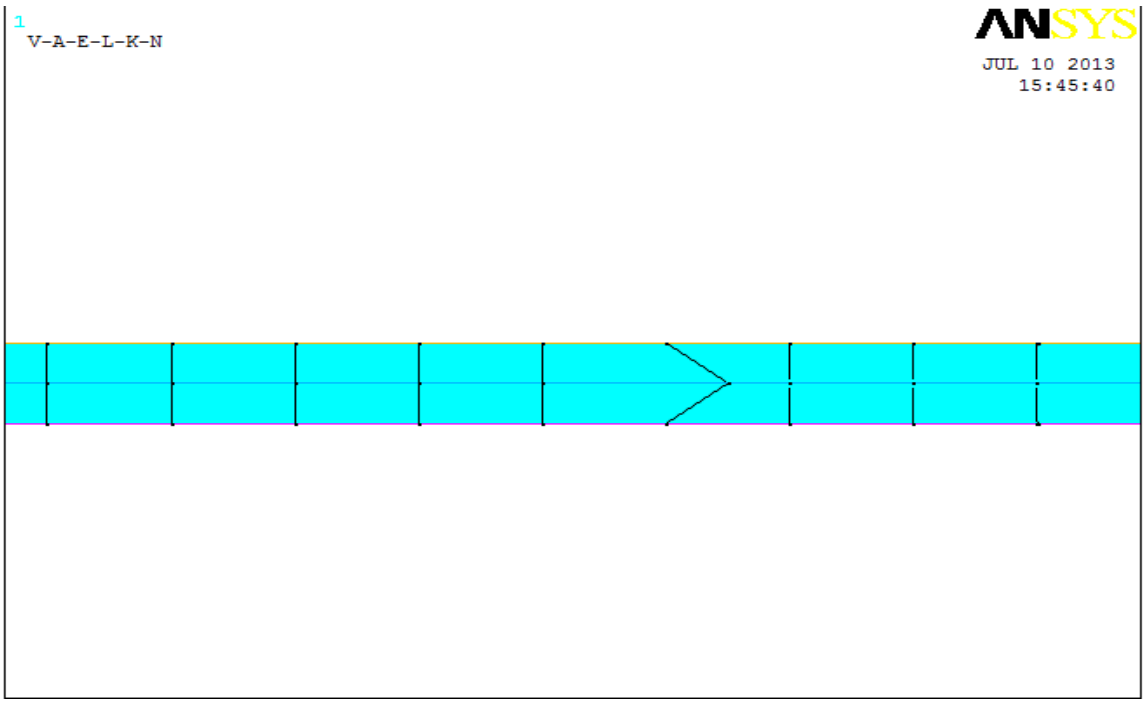

Figure 5.2 Illustration of Crack Tip Moved by a+Δa

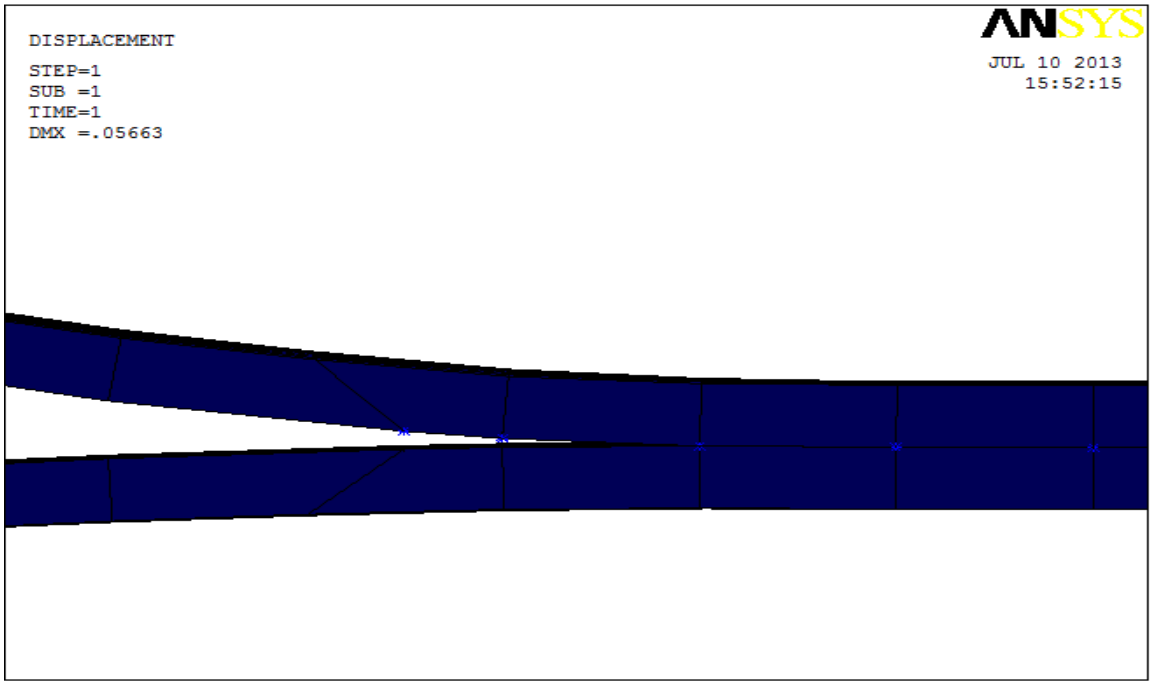

Figure 5.3 Illustration of Crack Tip Front for a+Δa

The above figures illustrate the method to evaluate strain energy release rate from ANSYS by using VCCT technique. Fig 5.1 depicts the crack tip when a load is applied and predicts the displacement and the nodal forces experienced by the DCB. Fig 5.2 explains the incremental change in crack length. Fig 5.3 shows the crack tip initiation and growth for the second analysis.

Chapter 6

Conclusions and Future Work

Analytical expression for calculating strain energy release rate of double cantilevered beam is developed. The expression is applicable for laminates in the temperature environment. An ANSYS model is also developed to validate the results obtained from the newly developed expression.

The results from the FEM and analytical approach depict that the elevation in temperature will not significantly alter the strain energy release rate, crack propagation enhancing the delamination or influencing effectively in DCB for IM7/8552 but the impact is significant if the temperatures are much higher. Theoretically, achieving the strain energy release rate at very high temperatures is practically not possible as the elevated temperature will affect the material properties which change its behavior to nonlinear. So, a detail study about the material non-linearity will give a clear picture to understand the SERR. The assumption of material properties remaining constant after the elevation of temperature really effect the values of strain energy release as the increase in temperature would change the material properties leading to soften the material which in fact will benefit to attain higher strain energy release rate values which supports to visualize a significant change. In general, materials can be time, rate and temperature dependent. So, analysis involving these dependency variables will fetch SERR which is much accurate.

The variation with the ply angle predicts that the inclusion of 90 degree plies will soften the laminate there by increasing the value of G different from only 0 degree laminate. The inclusion of 45 degree plies clearly demonstrates the importance of Mode III. As the prediction is 'G_{TOTAL}' the parametric study facilitated to understand the underlying effects and other major contributions for the higher G values. The symmetric and un-symmetric layups gives the insight of

the variation in SERR due to symmetry in laminate. Also, a similar kind of approach can be observed in evaluating the hygro-thermal effects on SERR.

The study related to evaluating G with different material properties reveal that the temperature effect can be effective for those materials which have higher thermal resistance. The brittle matrix will generally have less SERR when compared to the thermoplastic. The T300/5208 has less SERR in temperature environment because of high internal energy in longitudinal direction causing more loss in SERR, in contrast to pure mechanical loading case.

As the entire thesis focuses on the delamination of double cantilever beam with general laminate which is a mixed-mode fracture receives minimum support from the thermal forces and moments resulting in changes not impressively different. A detailed analysis with Mode II and Mode III will provide a complete understanding of the delamination in temperature environment. The present work is executed on fundamental model of double cantilever beam and can be extended to DCB with curvatures induced. This will significantly drives more as the temperatures will induce more curvatures which cannot be suppressed. The crack front is considered to be linear for this research which is not a necessary condition. So, evaluating the SERR for a crack tip front being curved can be considered for the further study.

APPENDIX A

Material Data

Material Critical Strain Energy Release Rate:

Material	Type of Test	Strain Energy release rate, G_{1c} (lb/in.)	Reference
T300/5208	DCB DCB	0.59 0.50	Ram Kumar and Whitcomb Wilkins
AS4/3501-6	DCB DCB HTDCB	1.13 1.08 1.08	Aliyu and Daniel Gillespie Daniel
AS4/3502	DCB	0.91	Whitney
T300/F-185	WTDCB	10.73	Daniel
AS4/PEEK	DCB DCB	9.99 8.33	Gillespie Prel

IM7/8552 data:

E1 = 2.335e7 Psi alp1=-0.0719e-6 / ^{O}C

E2 = 1.650e6 Psi alp2= 21.2e-6 / ^{O}C

v12 = 0.32

G12 = 0.74e6 Psi

T300/5208 data:

E1 = 33e6 Psi alp1=-0.4e-6 / ^{O}F

E2 = 2.2e6 Psi alp2=6.7e-6 / ^{O}F

v12 = 0.28

G12 = 4e6 Psi

AS4/PEEK data:

E1 = 19.9e6 Psi alp1=-0.1e-6 / ^{o}F

E2 = 1.27e6 Psi alp2=13.3e-6 / ^{o}F

v12 = 0.28

G12 = 0.73e6 Psi

APPENDIX B

Ansys Program

Ansys Program:

```
/NOPR
KEYW,PR_SET,1
KEYW,PR_STRUC,1
KEYW,PR_THERM,0
KEYW,PR_FLUID,0
KEYW,PR_ELMAG,0
KEYW,MAGNOD,0
KEYW,MAGEDG,0
KEYW,MAGHFE,0
KEYW,MAGELC,0
KEYW,PR_MULTI,0
KEYW,PR_CFD,0
/GO
!*
!*
/PREP7
!*
ET,1,PLANE182
!*
ET,2,SOLID185
!*
KEYOPT,1,1,0
```

```
KEYOPT,1,3,0
KEYOPT,1,6,0
!*
KEYOPT,2,2,0
KEYOPT,2,3,1
KEYOPT,2,6,0
!*
!*
!*
!*
!*
!*
MP,EX,1,2.335E7
MP,EY,1,1.65E6
MP,EZ,1,1.65E6
MP,GXY,1,0.74E6
MP,GXZ,1,0.74E6
MP,GYZ,1,0.568E6
MP,PRXY,1,0.32
MP,PRXZ,1,0.32
MP,PRYZ,1,0.45
*SET,KOPEN  , 1.E6
TB,CZM,2,1,1,CBDE
TBDATA,1,1.7,0.28,,,1.E-8
sect,1,shell,,top
```

secdata, 0.005,1,0,3

secdata, 0.005,1,0,3

secdata, 0.005,1,0,3

secdata, 0.005,1,0,3

secdata, 0.005,1,0,3

secdata, 0.005,1,0,3

secdata, 0.005,1,0,3

secdata, 0.005,1,0,3

secdata, 0.005,1,0,3

secdata, 0.005,1,0,3

secdata, 0.005,1,0,3

secdata, 0.005,1,0,3

secdata, 0.005,1,0,3

secdata, 0.005,1,0,3

secdata, 0.005,1,0,3

secdata, 0.005,1,0,3

secdata, 0.005,1,0,3

secoffset,MID

secf,%KOPEN%, 0

seccontrol,,,, , , ,

sect,2,shell,,bottom

secdata, 0.005,1,0,3

secdata, 0.005,1,0,3

secdata, 0.005,1,0,3

secdata, 0.005,1,0,3

secdata, 0.005,1,0,3

secdata, 0.005,1,0,3

secdata, 0.005,1,0,3

secdata, 0.005,1,0,3

secdata, 0.005,1,0,3

secdata, 0.005,1,0,3

secdata, 0.005,1,0,3

secdata, 0.005,1,0,3

secdata, 0.005,1,0,3

secdata, 0.005,1,0,3

secdata, 0.005,1,0,3

secdata, 0.005,1,0,3

secoffset,MID

secf,%KOPEN%, 0

seccontrol,,,, , , ,

BLC4, , ,6,2.5

ADELE, 1

FLST,2,4,4,ORDE,2

FITEM,2,1

FITEM,2,-4

LDELE,P51X

FLST,2,4,3,ORDE,2

FITEM,2,1

FITEM,2,-4

KDELE,P51X

```
GPLOT
BLC4, , ,6,2
/AUTO,1
/REP,FAST
AATT,      1, ,   1,      0,   1
TYPE,   1
MAT,      1
REAL,
ESYS,      0
SECNUM,   1
!*
FLST,2,1,5,ORDE,1
FITEM,2,1
AESIZE,P51X,0.1,
MSHAPE,0,2D
MSHKEY,0
!*
CM,_Y,AREA
ASEL, , , ,       1
CM,_Y1,AREA
CHKMSH,'AREA'
CMSEL,S,_Y
!*
AMESH,_Y1
!*
```

```
CMDELE,_Y
CMDELE,_Y1
CMDELE,_Y2
!*
/UI,MESH,OFF
FLST,5,1071,1,ORDE,7
FITEM,5,2
FITEM,5,12
FITEM,5,-81
FITEM,5,83
FITEM,5,-132
FITEM,5,332
FITEM,5,-1281
NSEL,R, , ,P51X
CM,CM_1,NODE
CMSEL,A,CM_1
/MREP,EPLOT
TYPE,   2
EXTOPT,ESIZE,1,0,
EXTOPT,ACLEAR,0
!*
EXTOPT,ATTR,0,0,0
MAT,1
REAL,_Z4
ESYS,0
```

```
!*
!*
VOFFST,1,0.04, ,
GPLOT
BLC4, , ,6,2
APLOT
TYPE,   1
MAT,      1
REAL,
ESYS,      0
SECNUM,   2
!*
FLST,2,1,5,ORDE,1
FITEM,2,7
AESIZE,P51X,0.1,
MSHAPE,1,3D
!*
CM,_Y,AREA
ASEL, , , ,      7
CM,_Y1,AREA
CHKMSH,'AREA'
CMSEL,S,_Y
!*
AMESH,_Y1
!*
```

```
CMDELE,_Y
CMDELE,_Y1
CMDELE,_Y2
!*
TYPE,   2
EXTOPT,ESIZE,1,0,
EXTOPT,ACLEAR,0
!*
EXTOPT,ATTR,0,0,0
MAT,1
REAL,_Z4
ESYS,0
!*
!*
VOFFST,7,-0.04, ,
!*
CM,_NODECM,NODE
CM,_ELEMCM,ELEM
CM,_KPCM,KP
CM,_LINECM,LINE
CM,_AREACM,AREA
CM,_VOLUCM,VOLU
MP,MU,2,0.01
MAT,2
MP,EMIS,2,7.88860905221e-031
```

```
R,3
REAL,3
ET,3,170
ET,4,175
R,3,,,1.0,0.1,0,
RMORE,,,1.0E20,0.0,1.0,
RMORE,0.0,0,1.0,,1.0,0.5
RMORE,0,1.0,1.0,0.0,,1.0
RMORE,10.0
KEYOPT,4,4,0
KEYOPT,4,5,0
KEYOPT,4,7,0
KEYOPT,4,8,0
KEYOPT,4,9,0
KEYOPT,4,10,2
KEYOPT,4,11,0
KEYOPT,4,12,5
KEYOPT,4,2,0
KEYOPT,3,5,0
! Generate the target surface
ASEL,S,,,7
CM,_TARGET,AREA
TYPE,3
NSLA,S,1
ESLN,S,0
```

```
ESLL,U
ESEL,U,ENAME,,188,189
NSLE,A,CT2
ESURF
CMSEL,S,_ELEMCM
! Generate the contact surface
NSEL,S,,,CM_1
CM,_CONTACT,NODE
TYPE,4
ESLN,S,0
ESURF
ALLSEL
ESEL,ALL
ESEL,S,TYPE,,3
ESEL,A,TYPE,,4
ESEL,R,REAL,,3
/PSYMB,ESYS,1
/PNUM,TYPE,1
/NUM,1
EPLOT
ESEL,ALL
ESEL,S,TYPE,,3
ESEL,A,TYPE,,4
ESEL,R,REAL,,3
CMSEL,A,_NODECM
```

```
CMDEL,_NODECM
CMSEL,A,_ELEMCM
CMDEL,_ELEMCM
CMSEL,S,_KPCM
CMDEL,_KPCM
CMSEL,S,_LINECM
CMDEL,_LINECM
CMSEL,S,_AREACM
CMDEL,_AREACM
CMSEL,S,_VOLUCM
CMDEL,_VOLUCM
CMDEL,_TARGET
CMDEL,_CONTACT
R,4,,,-1000000, ,,
RMORE,,,, ,,-1000000
RMORE,,,, ,,
RMORE,,,, ,,
RMORE,,,,,,
RDEL,4
RMODIF,3,3,-KOPEN
RMODIF,3,12,-KOPEN
FINISH
/SOL
FLST,2,2,5,ORDE,2
FITEM,2,4
```

```
FITEM,2,10
!*
/GO
DA,P51X,UX,
GPLOT
NPLOT
FLST,2,20,1,ORDE,2
FITEM,2,62
FITEM,2,-81
!*
/GO
D,P51X, , , , , ,UY, , , , ,
FLST,2,3,1,ORDE,3
FITEM,2,72
FITEM,2,1354
FITEM,2,3916
!*
/GO
D,P51X, , , , , ,UZ, , , , ,
GPLOT
LPLOT
FLST,2,1,4,ORDE,1
FITEM,2,20
!*
/GO
```

```
GPLOT
GPLOT
NPLOT
LPLOT
NPLOT
FLST,2,21,1,ORDE,4
FITEM,2,1282
FITEM,2,1285
FITEM,2,1423
FITEM,2,-1441
!*
/GO
F,P51X,FZ,3
FLST,2,21,1,ORDE,4
FITEM,2,3844
FITEM,2,3847
FITEM,2,3985
FITEM,2,-4003
!*
/GO
F,P51X,FZ,-3
/STATUS,SOLU
SOLVE
FINISH
```

MATLAB Code:

To Find ABD MATRIX:

```
function [compgen,abd] = ABDgen(h,E1,E2,v12,G12,th)
% [ A,B,D] = ABDgen(h,E1,E2,v12,G12,th)
% This function generates  Compliance Matrices
% h - vector containing ply boundaries
% E1,E2, v12, G12 - material properties
% th - vector containing ply angles

n = size(h);
n = n(1) - 1;
s=mats(E1,E2,v12,G12);
Q12=s^-1;
Qxy=zeros(3,3,n);
A = zeros(3,3);
B = zeros(3,3);
D = zeros(3,3);

for m=1:n
Qxy(:,:,m)=rotsigma(-th(m))*Q12*rotepsi(th(m));
A = A + Qxy(:,:,m)*(h(m+1) - h(m));
B = B + 0.5*Qxy(:,:,m)*(h(m+1)^2 - h(m)^2);
D = D + 0.33333*Qxy(:,:,m)*(h(m+1)^3 - h(m)^3);
end
```

```
compgen=[A B;B D]
x=mat2cell(compgen,[3 3],[3 3]);
% celldisp(x);
A=x{1,1};
B=x{1,2};
D=x{2,2};
format long
abd=inv(compgen)
end
```

To Find Thermal Forces and Moments:

```
function [Thermgen] = therm_gen(h,E1,E2,v12,G12,th,alp1,alp2,alp12,dT)
% [ A,B,D] = ABDgen(h,E1,E2,v12,G12,th)
% This function generates  Compliance Matrices
% h - vector containing ply boundaries
% E1,E2, v12, G12 - material properties
% th - vector containing ply angles
% %  Perfect Program
n = size(h);
n = n(1) - 1;
s=mats(E1,E2,v12,G12);
Q12=s^-1;
Qxy=zeros(3,3,n);
Nt=zeros(3,1);
Mt=zeros(3,1);
for m=1:n
```

```
Qxy(:,:,m)=rotsigma(-th(m))*Q12*rotepsi(th(m))

Nt= Nt+(Qxy(:,:,m)*alpxy(alp1,alp2,alp12,th(m))*dT*(h(m+1) - h(m)));

Mt= Mt+0.5*(Qxy(:,:,m)*alpxy(alp1,alp2,alp12,th(m))*dT*(h(m+1)^2 - h(m)^2));


end

Thermgen=[Nt;Mt]
```

References

[1] G.M. Nawaz, “Delamination in Advanced Composites,” Technomic Publishing Company, 1991.

[2] J.M. Whitney, C.E. Browning, W. Hoogsteden, “A Double Cantilevered Beam Test for Characterizing Mode I Delamination of Composite Materials,” Journal of Reinforced Plastic Composites, Vol. 7, pp. 297, 1982.

[3] A.S.D. Wang and F.W. Crossman, “Initiation and Growth of Transverse Cracks and Edge Delamination in Composite Laminates, Part 1: An Energy Method,” Journal of Composite materials, Vol. 14, 1980, pp. 71-87.

[4] T.K. O’Brien, “Characterization of Delamination Onset and Growth in a Composite Laminate”, Damage in Composite Materials, ASTM STP 775 (1982), p. 140.

[5] W.S. Chan and A.S.D. Wang, “Effects of the 90 Degree Ply in Matrix Cracks in Composite Laminates,” Composite Science and Technology, 38, 143-157, 1990.

[6] G.R. Irwin, “Fracture, Handbuch der Physik,” Vol. 6, Springer-Verlag, pp. 551, 1958.

[7] E.F. Rybicki and M.F. Kanninen, “A Finite Element Calculation of Stress Intensity Factors by Modeling Crack Closure Integral,” Engineering Fracture Mechanics, Vol. 9, pp. 931-938, 1977.

[8] “Ansys Reference Manual-Ansys Guide 12.1,” ANSYS, Inc.

[9] “Structural Analysis Guide Release 5.5” ANSYS, Inc.

Biographical Information

Venkata Naga Ravitej, Sankarabatla received his bachelor's degree in Aeronautical engineering from Institute of Aeronautical Engineering, India 2011.He joined University of Texas at Arlington in August 2011, for his master's program in Aerospace Engineering. He always wanted to expertise in Aerospace Structures. He expressed his desire to work under Dr. Chan in the field of composite structures as this would be challenging and helps him in enhancing the skill in structures.

He also worked in Dr. Chan's Composite Lab on project in association with Bell Helicopters. He wants to keep pace with latest technology in structures and gain some Industrial experience before he establishes himself.